Quaternary Science Reviews 32 (2012) 1–24

Contents lists available at SciVerse ScienceDirect

Quaternary Science Reviews

journal homepage: www.elsevier.com/locate/quascirev

A deglacial model for Antarctica: geological constraints and glaciological modelling as a basis for a new model of Antarctic glacial isostatic adjustment

Pippa L. Whitehouse [a,*], Michael J. Bentley [a], Anne M. Le Brocq [b]

[a] Department of Geography, Durham University, South Road, Durham, DH1 3LE, UK
[b] Geography, College of Life and Environmental Sciences, University of Exeter, Rennes Drive, Exeter, Devon, EX4 4RJ, UK

ARTICLE INFO

Article history:
Received 13 June 2011
Received in revised form
15 November 2011
Accepted 17 November 2011
Available online 22 December 2011

Keywords:
Antarctica
Last Glacial Maximum
Deglaciation
Ice-sheet model
Geological data
Glacial isostatic adjustment

ABSTRACT

We present a new reconstruction of the Antarctic Ice Sheets between 20 ka BP and the present day. Our reconstruction is derived using a numerical model to generate a physically-consistent ice surface across the whole of the continent. We define the extent of the ice sheet at five time slices; 20, 15, 10, 5 and 0 ka BP, assuming an equilibrium state for the 20 ka BP time slice, and a transient state for the deglacial time slices. The evolution of the ice sheet within the numerical model is driven by variations in temperature, accumulation rate, and relative sea level. In order to reconstruct the concave profile of the ice sheet in marine-grounded regions, such as the Ross and Weddell Seas, we force our model to develop channels of faster flow by defining greater basal sliding along the trajectory of former ice streams. We find a strong dependence upon the basal sliding parameters, and also the position of the grounding line. We use an extensive data base of geological and glaciological data to constrain our ice-sheet reconstruction. Grounding-line extent is prescribed from marine geological data and we test ice-sheet thickness against onshore geological data at 62 sites. Of the five time slices considered, our 20 ka BP reconstruction is the best constrained by data and has an RMS misfit of 147.6 m when compared to observations of ice thickness change between 20 ka BP and the present day. Across all time slices there are large regions of the ice-sheet which are poorly constrained, especially after 20 ka BP. We estimate the spatial distribution of uncertainty in our ice-sheet reconstruction, and note that the solutions are least reliable in regions of complex topography. We predict that the Antarctic Ice Sheets contributed 9 ± 1.5 m of eustatic sea level to the global ocean between 20 ka BP and the present, and our reconstruction with minimum misfit contributes ~8 m eustatic sea level during this period. These values, which we argue are an upper bound, are lower than many previous estimates. The reconstructed pattern of ice unloading can serve as a new input for glacial isostatic models.

1. Background and rationale

The deglacial history of Antarctica is poorly understood in comparison to the other large Late Quaternary ice sheets. This has implications for a number of objectives including contextualising observations of present-day ice-sheet changes, understanding the response of the Antarctic Ice Sheets (AIS) to external forcing, and quantifying the Antarctic contribution to eustatic sea-level change since the Last Glacial Maximum (LGM). With regard to the first of these, correcting contemporary geodetic measurements for glacial isostatic adjustment (GIA) is of particular interest. GIA is driven by past ice loading, and its modelling requires accurate reconstruction of the deglaciation history (Ivins and James, 2005; Chen et al., 2006; Bentley, 2010). Datasets are available which provide constraints on ice-sheet history, however, there is a wide diversity of data types and their interpretation, in many cases, is not straightforward. As a result, synthesising the observational constraints into a compilation suitable for model testing is a major undertaking. There have been previous attempts to develop reconstructions of the LGM AIS from field data (Denton and Hughes, 2002; Heroy and Anderson, 2005) but the model proposed by Ivins and James (2005) is the only major synthesis of the full Antarctic deglacial history from LGM-to-Present that we are aware of. This was a major advance and the resulting ice loading history (usually called IJ05) has since been widely adopted in GIA models and used to remove the contribution of past ice-sheet changes embedded in geodetic observations, thus better isolating the signal associated with contemporary changes (Chen et al., 2006, 2008, 2009; Ramillien et al., 2006; Velicogna and Wahr, 2006; Velicogna, 2009). Other Antarctic ice histories have been input into GIA models, for example: the Antarctic component

* Corresponding author.
E-mail address: pippa.whitehouse@durham.ac.uk (P.L. Whitehouse).

0277-3791/$ – see front matter © 2011 Elsevier Ltd. All rights reserved.
doi:10.1016/j.quascirev.2011.11.016

of ICE-5G (Peltier, 2004), ANT3 (Nakada and Lambeck, 1988), and various forms of the model of Huybrechts (Huybrechts, 2002; Bassett et al., 2007; Sasgen et al., 2007). However, none of these are as closely tied as IJ05 to the glacial geological field evidence in Antarctica.

While the IJ05 model is generally regarded as the most accurate deglacial history used in current GIA models, it has two limitations. Firstly, no information regarding the flow physics of ice sheets was applied in its development; rather, the model comprises an array of circular disks arranged to best-fit observational constraints on ice extent. This array is then smoothed using a spherical harmonic representation. This approach necessarily makes assumptions, which may not be physically plausible, about ice loading in areas with minimal data constraints. Secondly, the IJ05 model did not incorporate all available glacial geologic and glaciological data, and since the model was developed there have been several new geological datasets collected, some of which may have significant implications for ice loading.

In this paper we build upon the work of Ivins and James (2005), synthesising the existing glacial geological and glaciological data and combining them with a numerical ice-sheet model in order to reconstruct the AIS at various time slices. Data sources include marine geological and geophysical data on grounded ice extent on the continental shelf, and terrestrial geological evidence of former ice-sheet thickness from nunataks or ice cores (Fig. 1). We incorporate relevant glacial geologic data that we are aware of, up to and including publications in March 2011. A numerical ice-sheet model is used to relate ice thickness and extent in well-constrained areas to those areas with little or no data. We specifically document the source of marine and terrestrial geological constraints on grounding line position and ice-sheet thickness. Moreover, we also document misfits between data and model predictions so as to quantify errors. Finally, we identify those areas or time intervals where constraints are poor, with the aim to stimulate and focus future field research.

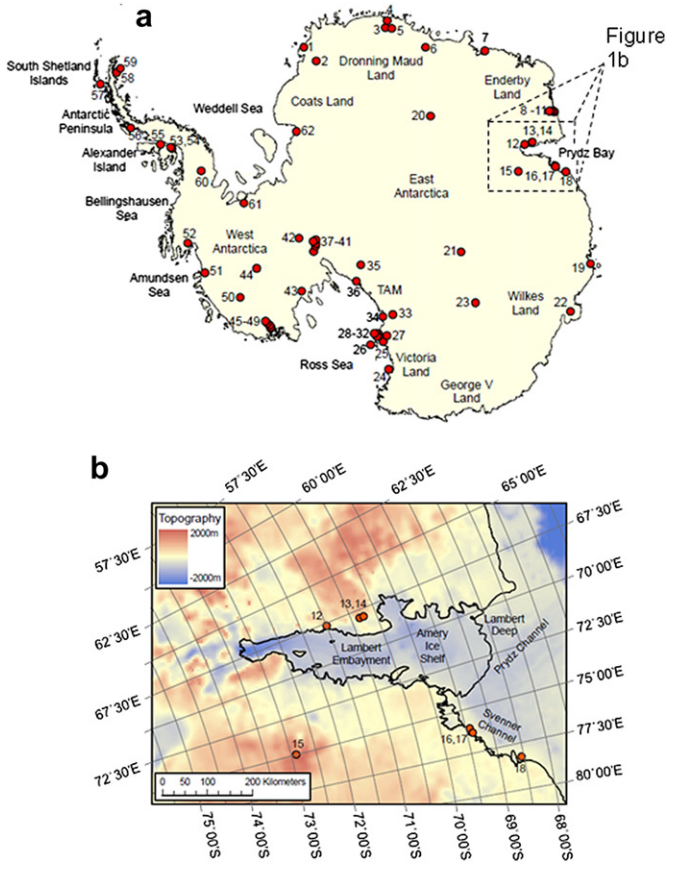

Fig. 1. (a) Map of Antarctica, showing present-day grounding line (derived from the MOA dataset (Haran et al., 2005 (updated 2006))). TAM = Transantarctic Mountains. Numbers refer to the data locations listed in Table 1. (b) Larger scale map of Prydz Bay.

In developing a loading history for use within a GIA model we do not seek to accurately capture the full dynamical behaviour of the ice sheet through time, but instead seek to reconstruct the geometry of the ice sheet at a series of discrete times. The overall aim is to develop a glaciologically-consistent Antarctic deglacial history that is closely tied to geological constraints on ice extent. Furthermore, we present a detailed description of our methodology so that our reconstruction is as transparent as possible, and provide the geological data in a form that makes their use straightforward for other modelling groups.

2. Approach and methods

In order to provide ice loading histories we adopt a time slice approach in which we attempt to describe the ice-sheet extent and thickness at a series of discrete times since the global LGM. Such an approach is comparable to published reconstructions of the Laurentide (Dyke and Prest, 1987) and Fennoscandian (Gyllencreutz et al., 2007) ice sheets, which have generally used 1000-year time slices. However, in the case of Antarctica the more limited availability of post-LGM data does not warrant such close time intervals and so we have adopted a 5000-year interval between time slices. This approach permits the later inclusion of higher resolution time slices, especially for key intervals such as across the time of meltwater pulse-1A (Clark et al., 2002; Bentley et al., 2010), or to describe Holocene ice-marginal fluctuations, as more data become available. We assume that the 20 ka BP time slice approximates to the peak ice-sheet extent of the global LGM (26.5–19 ka BP; Clark et al., 2009), with global ice-sheet retreat starting 20–19 ka BP. Of course, it is unlikely that the local LGM was reached synchronously throughout Antarctica (Anderson et al., 2002), and it may not have occurred precisely at 20 ka BP. We explore the implications of this assumption relating to the LGM timing for our model in the discussion.

Our new deglacial model for Antarctica is generated using the Glimmer ice-sheet model (Rutt et al., 2009), constrained by geological and glaciological data. For each time slice a mask is constructed to define the grounding line position: the maximum permitted lateral extent of grounded ice generated by the numerical model. The mask is based on marine geological and geophysical evidence from the continental shelf (See Fig. S1, Table S1 in Supporting Online Material; SOM). The shape of this mask exerts a dominant control upon the form of the resulting ice sheet (Saito and Abe-Ouchi, 2010). The second forcing which drives the temporal evolution of the ice sheet is the climate. For each time slice, the present-day surface temperature distribution is linearly shifted according to the palaeo-temperature record, as derived from East Antarctic ice cores (Petit et al., 1999; Jouzel et al., 2007). The present-day distribution of accumulation rates is also linearly scaled for each time slice, using the linear relationship between surface temperatures and accumulation rates (Muszynski and Birchfield, 1985). In addition, variations in surface temperature due to changes in the elevation of the ice-sheet surface during the model run are implemented using a linear lapse rate. Finally, past sea-surface heights are prescribed for each time slice. Other components of the numerical model are tuned during the process of attempting to reproduce the geometry of the present-day and palaeo ice sheets. Predictions for the present day are tested against

surface DEM data (Bamber et al., 2009; Le Brocq et al., 2010). Predictions for earlier time slices are tested against observations of past ice heights at locations in the interior of Antarctica. These data, and data relating to the lateral extent of the ice sheet, are discussed in the next section.

3. Glacial geological and glaciological data

Data on the former extent of the AIS come from a diverse range of sources, as summarised in Table 1 and S1. Amongst the most commonly collected and widely available are the marine geophysical and marine geological datasets collected from the Antarctic continental shelf. These include geophysical evidence of past grounded ice such as reflection seismic profiles and side-scan sonar, both of which tend to reveal over-consolidated subglacial sediments (tills) or erosional unconformities that demonstrate glacial overriding. These data have been collected for several decades and there is now reasonable coverage in the Ross Sea, western Antarctic Peninsula continental shelf, and Prydz Bay; growing amounts in the Amundsen Sea and around parts of East Antarctica; but much less in the Weddell Sea and some parts of the East Antarctic continental shelf. More recently multibeam (swath) bathymetry has become an effective tool for mapping past ice-sheet extent. The advent of such techniques has allowed detailed mapping of former grounding lines in several areas (Anderson et al., 2002) but the technique is relatively recent and only a few ships have been equipped with the instrumentation so, as with seismics and side-scan sonar, there are still prominent data gaps, particularly in the Weddell Sea and parts of the East Antarctic continental shelf.

The geophysical data delineate former ice-sheet extent but determining the timing of grounding line retreat requires marine sediment core retrieval. These sediments can be retrieved from within former ice-sheet limits and radiocarbon dating used to infer the timing of the transition from sub ice-sheet deposition to open water conditions (sometimes after a transition through sub-ice shelf sedimentation), and thus the retreat history. Dating of Antarctic marine sediment is challenging and requires careful selection of sample material (e.g., see the reviews of Heroy and Anderson (2007) and Hall et al. (2010)).

Onshore data, useful for constraining ice-sheet position or thickness (Fig. 1, Table 1), are based on a diverse set of techniques. Arguably the most common approach nowadays is to use the presence of moraine 'garlands' or scatters of erratic boulders on nunataks to infer the presence of formerly thicker ice. The timing of ice-sheet thinning comes primarily from cosmogenic surface exposure dating of the glacially-deposited materials, or of glacially-eroded bedrock (Stone et al., 2003; Sugden et al., 2005). Radiocarbon dating of organic remains has also been widely used around the continent, particularly prior to the application of cosmogenic dating techniques and especially on biological indicators of 'no-ice'. Such deposits have included remains of marine birds and mammals preserved in raised beaches (Hall and Denton, 1999), stomach oil deposits from nesting petrels (Hiller et al., 1988), lacustrine sediments (Hodgson et al., 2001), and algal remains in former ice-marginal ponds (Bockheim et al., 1989) and pro-glacial lakes (Hall et al., 2001). In all these cases the date of 'no-ice' material gives a minimum age for the retreat of ice from that site.

Glaciological data can also provide constraints on ice-sheet thickness. Ice cores have been used to infer former ice-sheet elevation using gas bubble analysis and isotopic analysis. These approaches are particularly important in the East Antarctic interior where there are few nunataks and so geological constraints are lacking. However, the data need to be interpreted with care since multiple processes affect the atmospheric and isotopic content of ice cores (Martinerie et al., 1994; Krinner et al., 2000). Radar layering coupled to ice cores or accumulation and flow models can also be used to infer the time at which ice domes or ice rises became independent ice dispersal centres after being overridden by formerly thicker ice sheets (Conway et al., 1999; Waddington et al., 2005). We draw on all of these data types in the compilation of our deglacial synthesis.

4. Ice-sheet modelling

We use the community ice-sheet model Glimmer (Rutt et al., 2009), run at a resolution of 20 km, to generate reconstructions of the AIS at specific times in the past. Each model run is defined by a set of initial conditions and a series of forcings or boundary conditions, as described below.

4.1. Initial conditions

Present-day bedrock topography and ice thickness are available at 5 km resolution (Le Brocq et al., 2010); we resampled the data onto a 20 km polar stereographic grid to aid computational efficiency, and used them to define initial conditions for the 20 ka BP time slice. The model is driven using appropriate forcings for this time slice (see below), and allowed to run for 50 ka in order to reach equilibrium. During a model run, the initial bedrock topography is assumed to be in equilibrium with the initial ice load. As the ice-sheet grows over time, the topography evolves according to the chosen isostatic model. Therefore, since the ice load and the bedrock topography evolve synchronously, the choice of initial conditions does not affect the final solution. For the post-20 ka BP time slices, including the present-day simulation that is used in the final reconstruction, the topography and ice-sheet thickness from the previous time slice are used as initial conditions, model forcings are set for the new time slice, and the model is only run for 5 ka; the time interval between each time slice. In reality, the AIS will not have reached an equilibrium state at any point during deglaciation due to the slow response time of the ice sheet (Huybrechts, 2002), and our method attempts to account for this by using a time-dependent numerical ice-sheet model which outputs a transient (as opposed to equilibrium) solution at the time interval of our choice.

4.2. Ice-extent masks

The lateral extent of the ice sheet at each time slice is prescribed using a mask (Fig. 2). Boundary conditions at the edge of marine-grounded regions are set to mimic the buttressing effect of an ice shelf, thus preventing the development of unrealistically large fluxes of ice across the grounding line (Le Brocq et al., 2011). We chose this method of prescribing ice extent over the use of a grounding line that is free to evolve in order to have control over the extent of the ice sheet at times when we have good geological constraints on the position of the grounding line.

Each mask is constructed primarily from published marine geological data (See Table S1, Fig. S1 and SOM for further details). The grounding line constraints have been compiled into extent masks for each time slice (Fig. 2). In some areas uncertainty in grounding line position is on the order of tens of kilometres, therefore we investigate the sensitivity of our model to grounding line position by generating two additional 20 ka BP ice-sheet reconstructions. These use grounding line masks that are shifted by 20 km onshore and 20 km offshore, respectively (20 km = one model grid cell).

Table 1
Ice thickness/elevation data. Sites are listed clockwise from the west coast of East Antarctica, and grouped into regions. EAIS = East Antarctic Ice Sheet; Ecore = ice core in East Antarctica; Ross = Ross Sea Embayment; Wcore = ice core in West Antarctica; WAIS = West Antarctic Ice Sheet; AP = Antarctic Peninsula; WS = Weddell Sea. All ice thickness/elevation changes are given in metres (m). Shaded boxes indicate no data. For terrestrial sites the lower and upper bounds refer to the change in ice thickness between the present-day and the palaeo time slice. For ice core sites the lower and upper bounds refer to the change in ice elevation between the present-day and the palaeo time slice.

Name	Site code	Region	Longitude (°E)[a]	Latitude (°S)[a]	20 ka BP time slice			15 ka BP time slice			10 ka BP time slice			5 ka BP time slice			Data type[e]	Source	Comments
					Lower ice thickness/ elevation difference[b]	Upper ice thickness/ elevation difference[c]	Likely ice thickness/ elevation difference[d]	Lower ice thickness/ elevation difference[b]	Upper ice thickness/ elevation difference[c]	Likely ice thickness/ elevation difference[d]	Lower ice thickness/ elevation difference[b]	Upper ice thickness/ elevation difference[c]	Likely ice thickness/ elevation difference[d]	Lower ice thickness/ elevation difference[b]	Upper ice thickness/ elevation difference[c]	Likely ice thickness/ elevation difference[d]			
Vestfjella	1	EAIS	−14.000	−73.170	360	700	–										UD	Jonsson (1988); Lintinen and Nenonen (1997)	Glacial striae and unweathered till indicate that ice was at least 360 m thicker at the LGM, but that the highest peaks (700 m above present ice surface) were not covered at the LGM.
Heimfrontfjella	2	EAIS	−11.000	−74.670	<250	250	–	<250	250	–	<250	250	–	<250	250	–	UD	Lintinen and Nenonen (1997); Hättestrand and Johansen (2005)	LGM ice ≤250 m thicker; undated supraglacial moraine up to 250 m above present ice surface inside the cirque and up to 100 m above present ice surface outside the cirque.
Insel Range	3	EAIS	11.600	−71.430	<80	80	–	<80	80	–	<80	80	–	<80	80	–	14C	Hiller et al. (1995)	Continuous snow petrel occupation since ~30 ka BP at a site 80 m above the present ice surface.
Schirmacher Oasis	4	EAIS	11.670	−70.750	0	0	–	0	0	–	0	0	–	0	0	–	14C, OSL	Krause et al. (1997)	Dated by OSL and C14 in lake: always ice free.
Untersee	5	EAIS	13.470	−71.350				<550	550	–	<550	550	–	<100	100	–	14C	Hiller et al. (1988)	Dates from snow petrel stomach oil; ice-free sites are used as upper elevation constraints on ice thickness; ice was below 1150 m a.s.l. by 15 ka BP, ice was below 700 m a.s.l. by 5 ka BP (present ice surface is at ~600 m).
Sør Rondane Massif	6	EAIS	25.000	−72.000	<30	30	–	<30	30	–	<30	30	–	<30	30	–	C	Moriwaki et al. (1991, 1992)	Local ice sheet thickening is limited to 30 m during the last 0.5 Ma.
Sôya coast/ Lutzow Holm Bay	7	EAIS	39.670	−69.250	350	>350	–	350	>350	–	350	>350	–	0	0	–	C	Hayashi and Yoshida (1994); Miura et al. (1998); Takada et al. (2003); Yamane et al. (2011)	Ice at least 350 m thick until 10 ka BP. Ice free by 5 ka BP.

Framnes Mountains, Brown Range	8	EAIS	62.370	−68.090	60	160	–	60	160	–	0	60	–	0	0	–	C	Mackintosh et al. (2007)	Locations exposed since 22 ka BP and 13 ka BP are used to define the upper and lower bounds of the 20 ka BP ice thickness difference, respectively. Back to present ice thickness by 5.1 ka BP.
Framnes Mountains, Dunlop Peak	9	EAIS	62.470	−67.950	172	192	–	172	192	–	172	192	–				C	Mackintosh et al. (2007)	Summit was ice free at 20 ka BP but covered at a point 30 m below the summit. Use summit height above present ice surface to determine ice thickness difference. Thinning took place after 10 ka BP.
Framnes Mountains, North Masson Range	10	EAIS	62.800	−67.780	329	>329	–	329	>329	–	100	100	–	0	0	–	C	Mackintosh et al. (2007)	North Masson Range completely covered at 20 ka BP; lower bound deduced from elevation of summit above current ice surface. Ice did not retreat until after 13 ka BP; Mackintosh et al (2007) give 250 m thinning between 12 and 10 ka BP and the final 100 m thinning between 10 and 7 ka BP.
Framnes Mountains, Mount Henderson	11	EAIS	63.050	−67.700	242	250	–	242	250	–	242	250	–	0	0	–	C	Mackintosh et al. (2007)	Lower bound deduced from the observation that Point 582 was still covered at 8.9 ka BP, upper bound deduced from the observation that the local maximum elevation of the covered surface is 250 m above the current ice surface. Back to present ice thickness by 6.6 ka BP.

(*continued on next page*)

Table 1 (*continued*)

Name	Site code	Region	Longitude (°E)[a]	Latitude (°S)[a]	20 ka BP time slice			15 ka BP time slice			10 ka BP time slice			5 ka BP time slice			Data type[e]	Source	Comments
					Lower ice thickness/ elevation difference[b]	Upper ice thickness/ elevation difference[c]	Likely ice thickness/ elevation difference[d]	Lower ice thickness/ elevation difference[b]	Upper ice thickness/ elevation difference[c]	Likely ice thickness/ elevation difference[d]	Lower ice thickness/ elevation difference[b]	Upper ice thickness/ elevation difference[c]	Likely ice thickness/ elevation difference[d]	Lower ice thickness/ elevation difference[b]	Upper ice thickness/ elevation difference[c]	Likely ice thickness/ elevation difference[d]			
Lambert Glacier, Fisher Massif	12	EAIS	67.670	−71.500	100	600	–										UD	Mabin (1991; 1992)	Undated upper moraine limit, assumed to be LGM; no information post-LGM.
Lambert Glacier, Radok Lake	13	EAIS	68.000	−70.830	0	0	–	0	0	–	0	0	–	0	0	–	C	Fink et al. (2006)	Not overidden by ice from the Lambert Embayment during the last glacial cycle, although note that Fink et al (2006) indicate that ice may have encroached from above.
Lambert Glacier, Amery Oasis	14	EAIS	68.000	−70.750	0	0	–	0	0	–	0	0	–	0	0	–	14C, C	Adamson et al. (1997); Fink et al. (2006)	Oasis not over-ridden during the last glacial cycle; the absence of a Holocene highstand in Beaver Lake indicates limited excess ice loading in this region during the last glacial cycle.
Grove Mountains	15	EAIS	75.000	−72.900	<0	0	–	<0	0	–	<0	0	–	<0	0	–	C	Liu et al. (2010); Lilly et al. (2010)	Ice not above current level during the last 20 ka, but ice surface could have been lower: only see long exposure bedrock ages near present-day ice surface; last time ice was thicker than present was prior to 50 ka; present-day elevation provides upper constraint on ice thickness for all time slices.
Stornes Peninsula	16	EAIS	76.110	−69.420	60	>60	–	60	>60	–	0	0	–	0	0	–	14C	Verleyen et al. (2004)	Ice-covered until 13.5 ka; highest point taken as a minimum; ice free from 13.5 ka BP onwards.

Larsemann Hills	17	EAIS	76.380	−69.380	0	0	–	0	0	–	0	0	–	0	0	–	14C	Burgess et al. (1994); Hodgson et al. (2001; 2005); Verleyen et al. (2005); Kiernan et al. (2009)	The Larsemann Hills are generally thought to have remained ice free during the LGM, but lake sediment from one site indicates that isolated locations may have been ice covered (Verleyen et al, 2005). We assume that the Larsemann Hills remained ice free for all of our time slices.
Vestfold Hills	18	EAIS	78.250	−68.550	158	700	–				0	0	–	0	0	–	14C	Fabel et al. (1997); Zwartz et al. (1998)	20 ka BP: lower limit from data, upper limit from GIA modelling of the LGM ice sheet. Ice-free by 11 ka BP.
Bunger Hills	19	EAIS	100.780	−66.280	<400	400	–	0	0	–	0	0	–	0	0	–	14C	Gore et al. (2001); Adamson and Colhoun (1992)	Gore et al (2001) claim that the Bunger Hills deglaciated at 20 ka BP and have stayed ice-free since then: this is adopted as the most likely scenario, but we use the earlier estimate from Adamson and Colhoun (1992) as an upper limit for the 20 ka BP time slice.
Dome Fuji ice core	20	Ecore	39.670	−77.320	−160	−150	–										IC	Parrenin et al. (2007)	Dating is based on a 1D flow model, palaeo-elevations are reconstructed using inverse modelling.
Vostok	21	Ecore	106.840	−78.440	−150	0	–										IC	Jouzel et al. (1989); Martinerie et al. (1994)	Ice core data suggest thinner ice at the LGM.
Law Dome	22	Ecore	112.800	−66.770	136	345	–	136	345	–							IC	Morgan et al. (1997); Delmotte et al. (1999)	Remained an independent ice dome – not overidden – but ice thickened by 136–345 m. Ice did not thin before 15 ka BP; rate of thinning unknown.
Dome C ice core	23	Ecore	123.380	−75.100	−160	−150	–										IC	Parrenin et al. (2007)	Dating is based on a 1D flow model; palaeo-elevations are reconstructed using inverse modelling.
Terra Nova Bay	24	Ross	164.500	−74.820	400	>400	–										14C	Baroni and Orombelli (1987)	

(continued on next page)

Table 1 (*continued*)

Name	Site code	Region	Longitude (°E)[a]	Latitude (°S)[a]	20 ka BP time slice			15 ka BP time slice			10 ka BP time slice			5 ka BP time slice			Data type[e]	Source	Comments
					Lower ice thickness/ elevation difference[b]	Upper ice thickness/ elevation difference[c]	Likely ice thickness/ elevation difference[d]	Lower ice thickness/ elevation difference[b]	Upper ice thickness/ elevation difference[c]	Likely ice thickness/ elevation difference[d]	Lower ice thickness/ elevation difference[b]	Upper ice thickness/ elevation difference[c]	Likely ice thickness/ elevation difference[d]	Lower ice thickness/ elevation difference[b]	Upper ice thickness/ elevation difference[c]	Likely ice thickness/ elevation difference[d]			
Hjorth Hill	25	Ross	163.620	−77.520	350	350	–										14C	Hall and Denton (2000)	
Cape Crozier	26	Ross	169.340	−77.500	710	710	–										14C	Denton and Marchant (2000)	
Ferrar Glacier	27	Ross	161.170	−77.960	0	0	–										C	Staiger et al. (2006)	
Mt Discovery west	28	Ross	164.740	−78.350	256	256	–										14C	Denton and Marchant (2000)	
Brown Peninsula west	29	Ross	165.260	−78.120	245	265	–										14C	Denton and Marchant (2000)	
Mt Discovery south-east	30	Ross	165.320	−78.420	327	519	–										14C	Denton and Marchant (2000)	
Brown Peninsula east	31	Ross	165.550	−78.130	340	360	–										14C	Denton and Marchant (2000)	
Minna Bluff	32	Ross	166.500	−78.500	590	637	–										14C	Denton and Marchant (2000)	
EAIS Plateau – Hatherton	33	Ross	154.500	−79.630	100	100	–										14C	Denton et al. (1989)	Data refer to the magnitude of thickening at the LGM, thinning rate unknown.
Hatherton Glacier grounding line	34	Ross	159.930	−79.791	800	1100	–										14C	Bockheim et al. (1989); Anderson et al. (2004)	Range of LGM increase in ice thickness at the grounding line is derived from both modelling and observations.
EAIS Plateau – Beardmore	35	Ross	163.000	−85.190	40	40	–										14C	Denton et al. (1989)	Data refer to the magnitude of thickening at the LGM, thinning rate unknown.
Beardmore Glacier	36	Ross	171.000	−83.750	1050	1050	–										14C	Denton et al. (1989)	Data refer to the magnitude of thickening at the LGM, thinning rate unknown.
Reedy Glacier (mouth, Cohen)	37	Ross	−136.220	−85.400	420	760	–	420	760	–	420	760	–	<105	105	–	C	Todd et al. (2010)	Maximum thickening given by ice height at Quartz Hills, minimum thickening given by highest buried nunatak at mouth (Langford). Configuration maintained until after 10 ka BP. Nunataks emerged 7.8–6.8 ka BP so height of lowest nunatak used as maximum for 5 ka BP.

Reedy Glacier (Quartz Hills)	38	Ross	−132.650	−85.900				210	250	–	<160	160	–	<120	120	–	C	Todd et al. (2010)	Maximum thickening achieved between 17.0 and 14.1 ka BP. Maximum recessional ice heights given during deglaciation.
Reedy Glacier (Caloplaca Hills)	39	Ross	−130.950	−86.090							111	123	–				C	Todd et al. (2010)	Maximum elevation attained between 14.7 and 10.2 ka BP; constraint is used for the 10 ka BP time slice. Ice thickness difference calculated from spot height on fig. 7 in Todd et al (2010).
Reedy Glacier (Hatcher Bluffs)	40	Ross	−126.090	−86.330										50	>50	–	C	Todd et al. (2010)	Minimum ice thickness: "at least 50 m ice height difference". Dates on erratics are 7.3 and 3.5 ka BP. Assume youngest age gives time of recession, so can use this as a minimum at 5 ka BP.
Reedy Glacier (Mims Spur)	41	Ross	−125.700	−86.040							<140	140	–				C	Todd et al. (2010)	Maximum elevation attained during 9.1–7.7 ka BP so upper limit of drift treated as a maximum for 10 ka BP.
Ohio Range	42	Ross	−114.000	−85.000	<125	125	–	<125	125	–	<125	125	–				C	Ackert et al. (2007); Hall (2009)	Thickening reached a maximum at 11.5 ka BP.
Siple Dome	43	Wcore	−148.820	−81.660	200	400	350	200	400	350	0	0	–	0	0	–	RL	Waddington et al. (2005); Price et al. (2007)	Data from Siple Dome ice core site (depth-age, layer-thickness, temperature) used to infer that the majority of thinning took place 14–15 ka BP. Close to present elevation by 10 ka BP.
Byrd Station	44	WCore	−119.520	−80.020	−200	300	–										IC	Raynaud and Lebel (1979); Jenssen (1983); Grootes and Stuiver (1986); Steig et al. (2001)	No constraint after LGM from ice core data.

(*continued on next page*)

Table 1 (*continued*)

Name	Site code	Region	Longitude (°E)[a]	Latitude (°S)[a]	20 ka BP time slice			15 ka BP time slice			10 ka BP time slice			5 ka BP time slice			Data type[e]	Source	Comments
					Lower ice thickness/ elevation difference[b]	Upper ice thickness/ elevation difference[c]	Likely ice thickness/ elevation difference[d]	Lower ice thickness/ elevation difference[b]	Upper ice thickness/ elevation difference[c]	Likely ice thickness/ elevation difference[d]	Lower ice thickness/ elevation difference[b]	Upper ice thickness/ elevation difference[c]	Likely ice thickness/ elevation difference[d]	Lower ice thickness/ elevation difference[b]	Upper ice thickness/ elevation difference[c]	Likely ice thickness/ elevation difference[d]			
Ford Ranges (coast/Rea)	45	WAIS	−145.600	−77.070	700	1400	–	700	1400	–	600	600	–	400	400	–	C	Stone et al. (2003)	Ice-sheet modelling implies that ice surface could have been at 1200−1500 m a.s.l. at the LGM (present ice surface is at ~100 m a.s.l.); peaks 700 m above the present ice surface were covered until 11 ka BP. Thinning constrained by cosmogenic dating.
Ford Ranges (Blades)	46	WAIS	−145.320	−77.160										290	290	–	C	Stone et al. (2003)	Constraints only from 7 ka BP onwards.
Ford Ranges (Fleming)	47	WAIS	−144.490	−77.250										180	180	–	C	Stone et al. (2003)	Constraints only from 5 ka BP onwards.
Ford Ranges (Darling)	48	WAIS	−143.330	−77.250							400	400	–	200	200	–	C	Stone et al. (2003)	Constraints only from 10 ka BP onwards.
Ford Ranges (Valkenburg)	49	WAIS	−142.110	−77.310	200	540	–	200	540	–	140	540	–	140	140	–	C	Stone et al. (2003)	Ice-sheet modelling implies that ice could have been at 1200 −1500 m a.s.l. at the LGM (present ice surface is at ~960 m a.s.l.); peaks 200 m above the present ice surface were covered until at least 11 ka BP. Thinning constrained by cosmogenic dating.
Mt Waesche	50	WAIS	−127.000	−77.200							<85	85	–				C	Ackert et al. (1999)	Lower moraine band (up to 45 m above the present ice surface) exposed since ~10 ka BP; limited data from the upper moraine band indicate that ice surface may have been up to 85 m thicker than present at the last highstand, which is assumed to have occurred ~10 ka BP, from ice-sheet modelling.

Turtle Rock	51	WAIS	−111.300	−75.370	334	>334	–				230	230	–	105	105	–	C	Johnson et al. (2008)	Ice-covered at the 20 ka BP. Thinning constrained by cosmogenic dating.
Hudson Mountains	52	WAIS	−99.150	−74.550	500	>500	–	500	>500	–	500	>500	–	0	0	–	C	Bentley et al., unpublished	Ice at least 500 m thicker at 15 ka BP and 10 ka BP.
Citadel Bastion	53	AP	−68.470	−72.020	465	>465	–	465	>465	–	<297	297	–	0	0	–	C	Hodgson et al. (2009)	Ice-covered at 20 ka BP; retreat started ~15 ka BP; col was ice-free by 10 ka BP; complete deglaciation shortly after.
Two Step Cliffs	54	AP	−68.250	−71.830	380	>380	–	380	>380	–	370	>370	–	0	0	–	C	Bentley et al. (2006)	Ice-covered at 20 ka BP; retreat started ~15 ka BP; final thinning after 7.4 ka BP; ice free by 7 ka BP.
Ablation Point massif (Ab. Pt at north)	55	AP	−68.550	−70.830	600	600	–	600	600	–	0	0	–	0	0	–	C	Bentley et al. (2006)	Grounding line at present position by 10 ka BP.
Pourquoi-Pas Island	56	AP	−67.470	−67.680	350	>350	–	350	>350	–	0	0	–	0	0	–	C	Bentley et al., unpublished	Ice-covered at 20 ka BP; retreat started ~15 ka BP; thinning complete by 10 ka BP.
Western Bransfield Basin	57	AP	−61.580	−63.370	1000	>1000	–										–	Canals et al. (2000)	Ice must have been at least 1000 m thick in this marine-based ice stream at the LGM (undated).
James Ross Island (Johnson Mesa)	58	AP	−57.750	−64.150	320	>320	–										C	Johnson et al. (2011)	Ice-covered at the LGM.
Seymour Island	59	AP	−56.630	−64.240	220	>220	–										C	Johnson et al. (2011)	Ice-covered at the LGM.
Behrendt Mountains	60	WS	−72.270	−75.320	300	>300	–	300	>300	–	<230	230	–				C	Bentley et al. (2006)	Site overriden until 15 ka BP. Retreat started ~15 ka BP. Thinning constrained by cosmogenic dating.
Ellsworth Mountains	61	WS	−82.000	−80.000	440	480	–	440	480	–	380	480	–	<170	170	170	C	Bentley et al. (2010)	Data from both the Southern Heritage Range and Marble Hills are amalgamated. Retreat started after ~15 ka BP.

(*continued on next page*)

Table 1 (*continued*)

Name	Site code	Region	Longitude (°E)[a]	Latitude (°S)[a]	20 ka BP time slice			15 ka BP time slice			10 ka BP time slice			5 ka BP time slice			Data type[e]	Source	Comments
					Lower ice thickness/ elevation difference[b]	Upper ice thickness/ elevation difference[c]	Likely ice thickness/ elevation difference[d]	Lower ice thickness/ elevation difference[b]	Upper ice thickness/ elevation difference[c]	Likely ice thickness/ elevation difference[d]	Lower ice thickness/ elevation difference[b]	Upper ice thickness/ elevation difference[c]	Likely ice thickness/ elevation difference[d]	Lower ice thickness/ elevation difference[b]	Upper ice thickness/ elevation difference[c]	Likely ice thickness/ elevation difference[d]			
Shackleton Range	62	WS	−30.000	−80.400	200	340	–										C	Kerr and Hermichen (1999); Fogwill et al. (2004); Hein et al. (2011)	Moraines on Mt Provender currently undated but assumed to be LGM by Fogwill et al (2004) and several Antarctic-wide reconstructions. Thinning rate unknown.

[a] Values are for location of field data; model uses nearest physically representative grid cell (i.e. not offshore for onshore sites). Model resolution is 20 km.
[b] Where lower bound not known then we indicate with '<', and plot as downward-pointing triangle in Figs. 5 and 6.
[c] Where upper bound not known then we indicate with '>', and plot as upward-pointing triangle in Figs. 5 and 6.
[d] Within the given max-min ranges the 'likely' elevation is the former ice elevation that we judge most probable from close reading of discussion or data plots in the original reference.
[e] C = Cosmogenic surface exposure dating; IC = ice core; 14C = radiocarbon dating (stomach oil, lacustrine algae, lake sediment, shells); OSL = optically stimulated luminescence; RL = radar layering and model; UD = undated geomorphological limit assumed to be 20 ka BP (LGM).

4.3. Climate inputs

Spatially-variable distributions of surface temperature and accumulation rate are used to drive the numerical ice-sheet model. For each time slice, the present-day surface temperature distribution (Comiso, 2000) is shifted by a uniform value according to palaeo-temperature reconstructions from the Vostok (Petit et al., 1999) and EPICA Dome C (Jouzel et al., 2007) ice cores. These reconstructions make use of the temperature dependence of the isotopic composition of precipitation (Jouzel et al., 2003; Blunier et al., 2004).

The shifted present-day temperature distribution is used to initiate each model run. Variations in surface temperature due to changes in the elevation of the ice-sheet surface during the model run are implemented using a linear lapse rate of 0.011°/m which is derived from the present-day temperature distribution of Comiso (2000). This is close to the dry adiabatic lapse rate, which has been shown to be a suitable approximation for temperature changes in the interior of East Antarctica (Magand et al., 2004). Lower lapse rates are found in West Antarctica (Magand et al., 2004), hence temperature changes in this region are likely to be over-estimated.

The present-day distribution of accumulation rates (Arthern et al., 2006) is scaled over time using the assumption that accumulation rates are linearly related to temperature, and that LGM accumulation rates were 50% lower than present (Lorius et al., 1984; Parrenin et al., 2004). The temperature shift and accumulation rate scaling factor for each time slice are given in Table S2.

By initiating each run with a linearly shifted version of the present-day distribution of these climate variables we inherently make the assumption that their spatial distribution has not changed over time. The limitations of this assumption are discussed in the SOM.

4.4. Basal sliding laws

We follow the approach of Le Brocq et al. (2011) and adopt different sliding laws for 'hard-bed' and 'soft-bed' regions

Fig. 2. Masks used to constrain ice-sheet thickness at the five time slices are shown in different shades of grey. The mask used to define regions of enhanced marine sliding is shown in red. The masks are overlain on bedrock elevation relative to present-day sea level. (For interpretation of the references to colour in this figure legend, the reader is referred to the web version of this article).

(Weertman, 1964; Budd et al., 1984; Huybrechts, 2002), defined to be the land-based and marine-based portions of the ice-sheet respectively, in an attempt to reproduce the convex-to-concave ice surface profiles observed across marine-grounded margins of the AIS. The parameters B_t and B_s are used to define the degree of sliding in the 'hard-bed' and 'soft-bed' regions, respectively (see SOM for further details). A range of values for these parameters are tested (see Table 2), and optimum values are determined prior to investigating the other variables listed in Table 2 due to the strong sensitivity of the solutions to the basal sliding parameters.

4.5. Ice-stream mask

In most of Antarctica, air temperatures are too low to cause surface melt to occur, except in a few regions of the Antarctic Peninsula; hence the majority of ice mass loss from the AIS is via ice streams, which transport ice to the calving front. Ice streams are a dominant feature of the observed velocity field, accounting for about 90% of ice transport in West Antarctica (Joughin and Tulaczyk, 2002), and their existence alters the profile of large regions of the ice sheet, for example in the Ross Sea, resulting in a concave rather than a convex profile between the ice divide and the grounding line. In soft-bed regions, Glimmer uses a spatially-uniform basal sliding parameter. Strong lateral velocity gradients observed at the margins of ice streams are reproduced by means of a thermal criterion, whereby sliding occurs only when the base of the ice is at the pressure melting point (see SOM). However, we have found that in order to reproduce observed velocity gradients satisfactorily we have had to alter the basal sliding parameter in ice stream areas. Therefore, in addition to the grounding line mask, we also define an ice-stream mask, within which B_s is defined to take a higher value wherever there is geological or glaciological evidence for current or former fast flow in marine-grounded areas (see SOM). We denote this enhanced sliding parameter B_s'. The extent of the ice-stream mask is held fixed for all time slices (Fig. 2), and the values of B_s' investigated are given in Table 2. We investigate the hypothesis that ice-stream basal conditions have varied over time (Vogel et al., 2003) and thus seek the optimum value of B_s' for each time slice.

Table 2
Parameter space for sensitivity experiments

Variable	Parameter space investigated							
Grounding line mask extent	[1]*'Best' grounding line for each time slice*				LGM mask extent varied by 20 km			
Climate inputs	*Vostok climate history*				EPICA Dome C climate history			
Soft-bed sliding parameter: B_s	0.5	*0.75*	1	1.25	1.5			
[2]Soft-bed sliding parameter: B_s'	1.5	*2*	2.5	3	*5*	*10*	15	25
Hard-bed sliding parameter: B_t	*1 x 10^{-5}*	5 x 10^{-5}	1 x 10^{-4}					
[3]Hard-bed sliding parameter: B_t'	5 x 10^{-4}	1 x 10^{-3}	*5 x 10^{-3}*					
Relative sea level	*Spatially variable sea surface height*				Uniform sea surface height (mean of spatially variable distribution)			
Isostatic model	*Strong earth model (D=10^{25} Nm, τ=3000 a)*				Weak earth model (D=10^{24} Nm, τ=1000 a)			
Geothermal heat flux	*Fox Maule et al. model*				Shapiro-Ritzwoller model			

[1] Values used in the 'best' solution are listed in italics
[2] Enhanced soft-bed sliding parameter for ice streams. The 20 ka, 15 ka and 10 ka experiments use B_s' = 10. The 5 ka experiments use B_s' = 5. The present-day experiments use B_s' = 2.
[3] Enhanced hard-bed sliding parameter for regions of high resolution topography

In addition to marine-based ice streams, fast flow also takes place along steeply-inclined glaciers draining through mountainous regions, such as the Transantarctic Mountains and the Antarctic Peninsula. In these regions a second type of mask is defined, within which B_t is defined to take a higher value. We denote this enhanced sliding parameter B_t'. We justify this approach not on the grounds of different basal parameters, but because our model resolution (20 km) is unable to resolve the narrow topographic troughs through which the glaciers drain. The values of B_t' investigated are given in Table 2, and a best-fit value is used for all experiments.

4.6. Relative sea-level

The Glimmer ice-sheet model has been modified here to permit the input of a spatially-variable sea-level forcing. Sea-level change takes place as a result of perturbations to two bounding surfaces; the geoid, or mean sea surface, and the solid earth. Glimmer automatically accounts for the deformation of the solid earth under a changing ice load. We account for perturbations to the mean sea surface height (geoid) by independently calculating *a priori* the predicted pattern of geoid height across Antarctica for each time slice, and inputting this as a spatially-varying initial condition (instead of Glimmer's globally uniform 'eustasy' parameter (Rutt et al., 2009)). In order to estimate past geoid heights we use the ICE-5G global deglaciation history (Peltier, 2004) and solve the sea-level equation using the methods outlined in Mitrovica and Milne (2003), incorporating an updated treatment of rotational feedback (Mitrovica et al., 2005).

The geoid signal includes a component due to variations in Antarctic ice mass change and the resulting redistribution of mantle material. This is a long wavelength signal, which is relatively insensitive to the details of the ice history, and we use this fact to justify our use of the ICE-5G model to determine the *a priori* distribution of geoid heights used in our ice model experiments. Once we have derived our Antarctic deglaciation history this will be incorporated into a global GIA model, and used to re-calculate the geoid height distribution around Antarctica. The GIA model results are presented separately in a companion paper (Whitehouse et al., in review): preliminary calculations suggest that close agreement between the geoid heights derived from the ICE-5G model and our new deglaciation history will validate our method. To investigate the importance of this model input, we consider both a spatially-varying sea-surface change (based on the ICE-5G model) and the spatial average of this signal (see Table 2).

4.7. Isostasy

The Glimmer ice-sheet model includes a simple approximation of the isostatic response of the solid Earth to changes in ice loading at each time step (Rutt et al., 2009). Following Le Meur and Huybrechts (1996) we use an elastic lithosphere with a flexural rigidity (D) of 10^{25} Nm, and a viscous mantle half space with a relaxation time (τ) of 3000 years. We also investigate a second Earth model, with a weaker lithosphere and a shorter relaxation time, that is more representative of the rheological properties of West Antarctica (Morelli and Danesi, 2004) (see Table 2).

4.8. Geothermal heat flux

Temperature boundary conditions at the upper surface of the ice sheet are varied between time slices; however, the geothermal heat flux distribution, which is used to calculate the basal temperature boundary condition, is fixed for all time slices. In our sensitivity experiments we use two spatially-variable geothermal

heat flux distributions (Shapiro and Ritzwoller, 2004; Fox Maule et al., 2005). There are no direct observations of geothermal heat flux within the interior of Antarctica; therefore both distributions are derived from proxy measurements. The Fox Maule et al. (2005) distribution is derived from magnetic field measurements, while the Shapiro and Ritzwoller (2004) distribution uses a seismic model.

5. Results

The grounding line extent masks (Fig. 2) provide a primary control on ice-sheet extent with climate forcing and basal sliding parameters largely dictating the shape of the ice-sheet surface. Here we discuss the fit of our model output to present-day ice-sheet thickness and onshore evidence of former ice-sheet thickness.

Experiments are carried out in order to sample the full parameter space given in Table 2. For the present-day reconstruction we investigate the sensitivity of the model to the basal sliding parameters, the isostatic model, and the geothermal heat flux distribution. For the palaeo time slices we investigate the sensitivity of the model to grounding line extent, climate history, relative sea level, the isostatic model, and the geothermal heat flux distribution. The ice-stream basal sliding parameter B'_s is tuned independently for each time slice due to the sensitivity of the solution to this variable. For the other sliding parameters, the values determined in the present-day reconstruction are also found to be optimum for the palaeo time slices, and so are held fixed in the results presented here. Test statistics (see SOM) are calculated for each experiment in order to determine the best-fit solution for each time slice.

5.1. Present-day ice-sheet reconstruction

The best fit to the present-day distribution of ice-sheet thicknesses in Antarctica (Le Brocq et al., 2010) is achieved using basal sliding parameters $B_s = 0.75$ and $B_t = 1 \times 10^{-5}$ for marine and land-based regions, respectively, an enhanced sliding parameter of $B'_s = 2$ in the ice-stream regions, and an enhanced sliding parameter of $B'_t = 5 \times 10^{-3}$ in regions of high relief topography. Optimum values for other variables are 10^{25} Nm for lithospheric rigidity, 1000 years for the asthenospheric relaxation time, and the basal heat flux distribution of Shapiro and Ritzwoller (2004). We compare our model output to present-day ice thickness observations, as opposed to ice surface elevations, since it is observations of ice thickness change that will be used to test the accuracy of the palaeo time slice reconstructions. For the modelled present-day ice sheet, the RMS misfit of the best-fit distribution is 241.2 m, the mean error is −6.1 m, and the excess ice volume compared to present is equivalent to −0.62 m eustatic sea level (ESL). We note, however, that there may be errors in the present-day ice-thickness distribution inferred from observations, particularly at the ice margin (Bamber et al., 2009).

The end product of this study is a reconstruction of AIS thicknesses between the LGM and the present day. This time-varying distribution will form the ice-loading component of a GIA model, and in such a model it is the change in ice thickness over time that dominates the GIA response in near-field regions. Any misfits in the reconstruction of the present-day ice sheet (Fig. 3) will not carry through to the GIA loading model since we just use the *change* in ice thickness, relative to the present-day model reconstruction, to define the change in ice loading over time. The exercise of modelling the present-day ice sheet is carried out to investigate the sensitivity of the model to the input parameters and to inform us about regions of the ice sheet where our model performs less well.

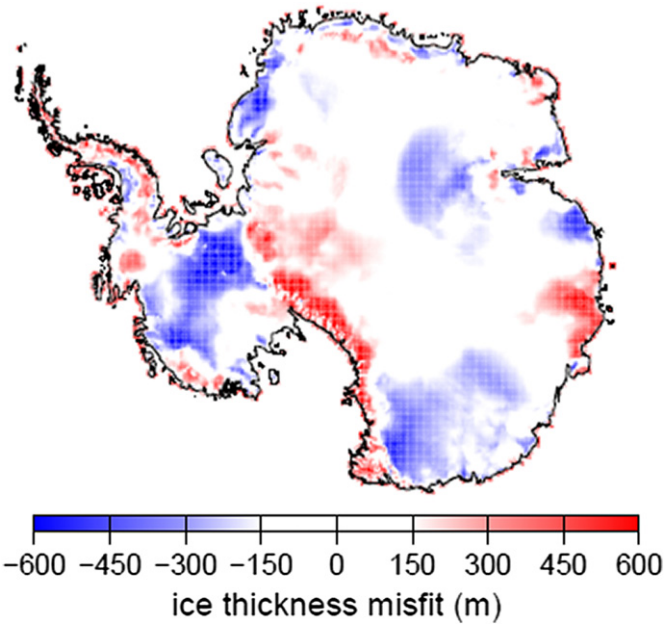

Fig. 3. Predicted minus observed ice thicknesses for the best-fit model to the present-day ice sheet.

In Fig. 3 we quantify the misfit in our ice-sheet reconstruction by plotting the distribution of model output minus observed ice-sheet thickness for the best-fitting present-day model. Observed ice thicknesses are given every 5 km by Le Brocq et al. (2010); we use the mean of all observed values within each 20 km model grid cell to determine the misfit within that cell. Blue areas imply that the model ice sheet is too thin, and red areas imply that the model ice sheet is too thick. Our model reconstruction overestimates present-day ice thicknesses in regions of high topographic variation, such as immediately behind the Transantarctic Mountains and along the Antarctic Peninsula, and underestimates ice-sheet thicknesses in many of the major marine-based basins in both East and West Antarctica. The model is weakly sensitive to the isostatic model and the heat flux distribution, but strongly sensitive to the basal sliding parameters (see SOM and Fig. S2). For example, decreasing the marine sliding parameter, B_s, in order to reduce the misfit inland of the Weddell Sea results in much thicker ice in the Ross Sea. The combination we have chosen minimises the misfit to the total ice volume and the ice thickness distribution. We do not seek to increase our modelling complexity further in order to rectify regional misfits; this is a task for regional modelling studies that employ more advanced numerical ice-sheet models. Our aim is not to understand the detailed dynamics of the ice sheet, but to reconstruct the geometry of ice-sheet mass change in a glaciologically-consistent manner.

5.2. Validating the palaeo ice-sheet reconstructions

Palaeo ice-sheet observations are compiled for each time slice reconstruction. We use 62 onshore geological and glaciological sites to validate our ice-sheet reconstruction, and these data are of two types (Table 1). In the first case, the data sites lie on exposed bedrock, and refer to a former position of the ice-sheet upper surface. Since the elevation of the bedrock site may have varied due to isostatic rebound, we use the change in ice thickness, relative to the present-day ice surface, as our test statistic. In the second case, the data are derived from ice cores, and refer directly to a palaeo-elevation. In this case we use the change in ice surface elevation as our test statistic; this is a combination of the change in ice

thickness and the isostatically-driven change in basal topography. The data may be maxima, minima, or absolute data, depending upon whether they were: (a) never covered by ice during the last glacial cycle, (b) definitely covered by ice at a given time during the last glacial cycle, or (c) mark the timing of ice retreat from a particular elevation, respectively. For absolute data that are listed without error bars we assume an observational elevation uncertainty of $\pm$10 m to account for the fact that the observations are extrapolated and compared with model predictions relating to a 20 $\times$ 20 km area (the area of a model grid cell). Ice elevations will vary substantially more than this locally, so by using $\pm$10 m we are deliberately conservative in our model validation. We quantify the misfit between model and field data by calculating the RMS, mean error, standard deviation of the mean error, and correlation coefficient of the weighted data set (see SOM).

5.3. Palaeo ice-sheet reconstructions

For the palaeo time slices, the Vostok temperature record and the Fox Maule et al. (2005) heat flux distribution lead to the best match between measured and modelled ice thickness changes. The solutions are only weakly dependent upon the sea surface height distribution, so we choose to use the spatially-varying sea surface height distribution for the final solution since we believe this to be physically more realistic. Finally, the experiments give a better fit to the data when the stronger earth model is used (lithospheric rigidity = 10^{25} Nm, asthenospheric relaxation time = 3000 years). The RMS misfit to the 20 ka BP palaeo ice-sheet observations for the best-fitting experiment is 147.6 m, the mean error is 48.8 m, the standard deviation of the error is 139.3 m, and the correlation coefficient is 0.56, which is statistically significant at the 99% confidence level. All these statistics take account of the weighting applied to the ice-sheet data (see SOM), and the degree of misfit decreases as the model approaches the present day (see Section 6).

We also generate a solution by taking the mean of all the 20 ka BP experiments (excluding those where the mask extent or basal sliding parameters are perturbed from their optimum values). This has an RMS misfit of 168.7 m, and gives a good fit to the data at many of the sites. However, in several regions there is a large degree of uncertainty associated with the input forcings, and while the best-fit solution generates ice thickness changes towards one end of the range, choosing the mean predicted ice thickness change results in large misfits in some regions, such as the Ross Sea (see Fig. 4a). Therefore we choose to use the best-fit solution for each time slice in our final ice-sheet reconstruction.

6. Model fit to glacial geological and glaciological data at all time slices

In the upper panels of Fig. 4a–d we plot the change in observed and predicted ice thicknesses between the present day and each palaeo time slice. A positive ice thickness difference value indicates thicker ice at some time in the past, and a negative value indicates thinner ice at some time in the past. The residual between observed and predicted ice thickness difference is plotted in the lower panels of Fig. 4 and in Fig. 5, where red colours indicate sites where our model produces an ice thickness change which is greater than observed, and blue colours indicate sites where our model produces an ice thickness change which is less than observed. Site numbers and names are listed in Table 1.

Our optimal model fits at least 85% of the sites to within 200 m of the observed change in ice thickness or elevation, and between 40% and 50% of the sites within the observational error bars. The weighted mean error gradually decreases from 48.8 m for the 20 ka BP time slice, through 35.7 m for the 15 ka BP time slice and 39.2 m for the 10 ka BP time slice, to 0.5 m for the 5 ka BP time slice, when the modelled ice thicknesses approach present-day values. The large weighted mean error for the 15 ka BP and 10 ka BP time slices reflects the difficulty of validating the ice-sheet configuration at discrete times during its deglacial phase. We discuss the sites in the order that they are plotted in Fig. 4, progressing clockwise around the continent from Dronning Maud Land (Fig. 1a).

6.1. East Antarctica

6.1.1. Geological data

With the exception of Schirmacher Oasis (site 4), 20 ka BP ice thickness changes in Dronning Maud Land are well reproduced by the model (Fig. 4a, sites 1–6; Fig. 5a). In the Insel Range (3) and the Sør Rondane Mountains (6) the change in ice thickness between 20 ka BP and the present is too large, while at Untersee (5) the change is too small in comparison to the limiting observational constraint. The data at these locations were collected from steep-sided nunataks which form part of a chain of mountains which protrude up to 1000 m above the surrounding ice sheet and form a topographical barrier which perturbs the flow of ice. The topographical detail of these regions is poorly represented by the 20 km resolution of our model, and the modelled change in ice thickness recorded at each grid point is representative of the regional change in ice surface, which may be different to actual changes recorded by geological data in complex topographic regions by several hundreds of metres. At Untersee, constraints on former ice thickness are determined from the dating of snow petrel stomach oil deposits (Hiller et al., 1988). The presence of dated organic material at a given height indicates that the ice sheet was below this level at that time. We use each dated constraint as an upper bound for the next time slice (e.g. material dated at 8 ka BP is used to determine an upper bound for the 5 ka BP time slice), but note that it is impossible to determine the precise height of the ice sheet at each time slice. Our model predictions all lie below these limiting constraints (site 5, Fig. 4a/d) in agreement with the data.

Luminescence and ^{14}C dating demonstrate that the 25 km $\times$ 3 km Schirmacher Oasis (4), which lies $\sim$100 m above sea level, has been ice free for at least 23 ka (Krause et al., 1997). This site lies in a topographically-flat region, at the boundary between the East Antarctic Ice Sheet (EAIS) and the Novolazarevskaya Ice Shelf, and it is not clear why it has remained ice free during this period. In our reconstruction of the present-day ice-sheet this site is covered by ice, and in all the 20 ka experiments the site is overridden by an additional 200–300 m ice (Fig. 4a, site 4). Due to the lack of further constraints on ice thickness change in this region, it is not yet possible to confirm whether our results are physically realistic. However, we note that an increase of ice thickness greater than a few hundred metres would create steep surface gradients around the oasis, rendering it impossible for such a small area to remain ice free, therefore we conclude that this region of the ice-sheet probably did not thicken by more than 200–300 m during the last glacial cycle. This magnitude of thickening is representative of the regional ice thickening in Dronning Maud Land produced by our model for the 20 ka BP time slice. Our model reconstruction predicts that the ice-sheet returned to its present-day thickness by 10 ka BP in this region of Antarctica, in agreement with the available data (Fig. 4c/d).

Larger changes in ice thickness are predicted at the margins of the ice sheet, in the region of grounding line advance and retreat. Along the Sôya coast, exposure dating and the maximum elevation of the coastal hills implies that the region was covered by at least 350 m of ice until 10 ka BP (Yamane et al., 2011); this observation was used to reconstruct the regional grounding line history, and is accurately reproduced by our model (Fig. 4a–c, site 7).

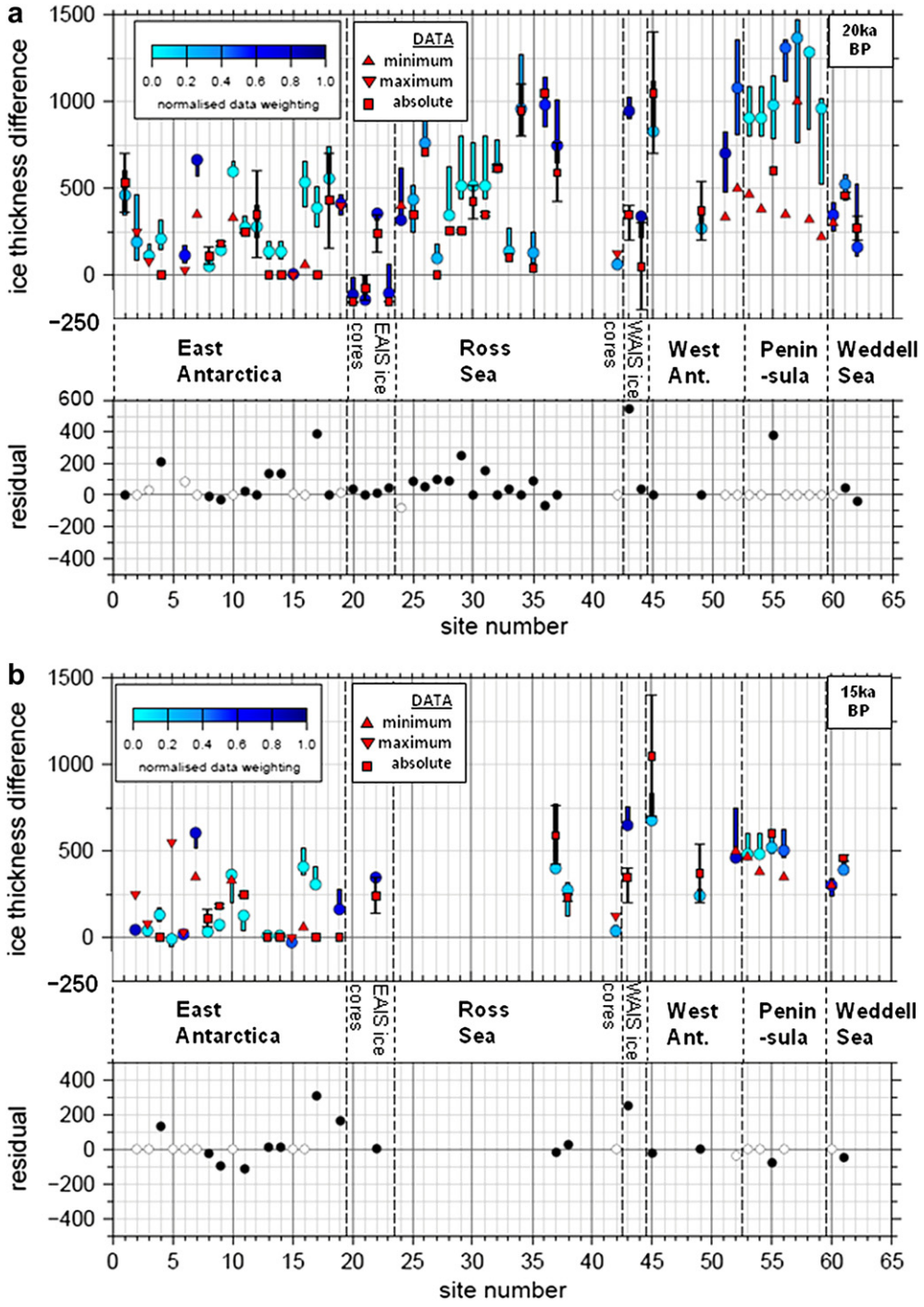

Fig. 4. Ice thickness change at the 62 data sites (see Table 1) at (a) 20 ka BP, (b) 15 ka BP, (c) 10 ka BP, and (d) 5 ka BP. Sites are plotted in order of increasing longitude, as listed in Table 1. In each upper plot we plot the change in ice thickness between the present day and the time slice reconstruction. Positive values indicate thicker ice at the time of the reconstruction. Observations are plotted in red with error bars in black. Upward-pointing triangles indicate a minimum limit on the change in ice thickness; downward-pointing triangles indicate a maximum limit on the change in ice thickness. Squares indicate an absolute change in ice thickness. Model predictions are plotted in blue; darker colours imply a greater weighting for that datum (see SOM). Blue circles mark the prediction from the best-fitting model for that time slice (see text), blue bars indicate the range of predicted ice thickness change at each data site for the parameter space given in Table 2 (ice extent and basal sliding parameters are held at optimum values). In each lower plot the residual of the predicted minus the observed value is plotted for the best-fit model. No misfit is recorded if the predicted value (blue circle) lies within the error bounds, or above/below a minimum/maximum-limiting datum. The misfit is plotted with an open circle for the case of the limiting data. (For interpretation of the references to colour in this figure legend, the reader is referred to the web version of this article.)

In the Framnes Mountains (8–11), cosmogenic dating permits tight constraints to be placed on the thinning history along a ~60 km transect through the mountains to the coast (Mackintosh et al., 2007). We caution that the 20 km resolution of our model limits our ability to model detailed ice flow in such a small region, but a comparison between the observations and our 20 ka BP reconstruction indicates that we accurately reproduce the magnitude of ice thickness change in this region during the last glacial cycle (Fig. 4a, sites 8–11). The position of the LGM grounding line and the timing of the initiation of retreat in this region are

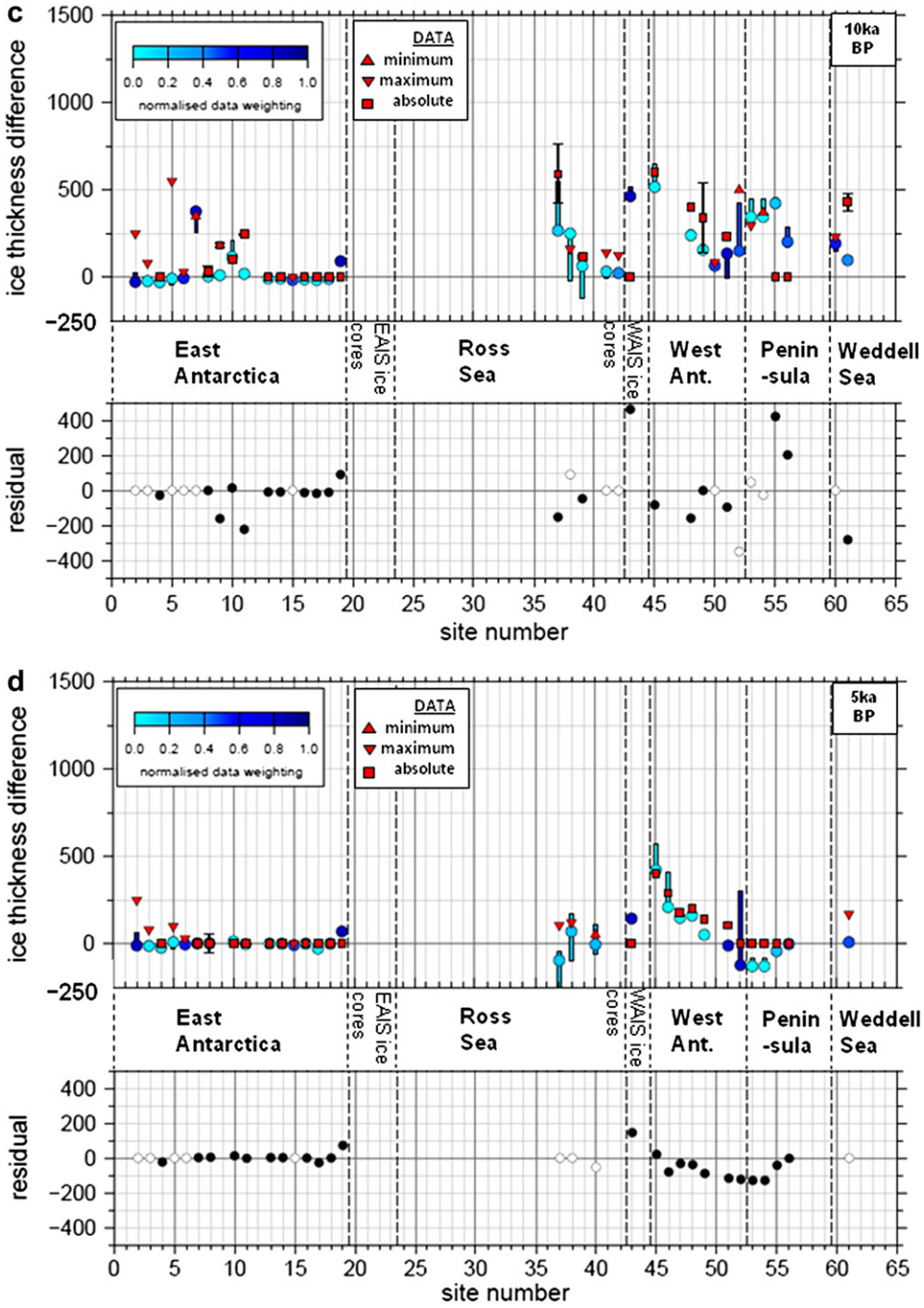

Fig. 4. (*continued*).

well-constrained from marine studies (Mackintosh et al., 2011), but the subsequent rate of grounding line retreat is poorly constrained. We find that our model reconstruction accurately reproduces the rate of thinning observed at the southern end of the transect (Brown Range, site 8), but that thinning is too rapid between 20 ka BP and 10 ka BP at the intermediate sites (Dunlop Peak and Mount Henderson, sites 9 and 11). This may be due to model limitations (e.g. spatial resolution, model physics) or the use of incorrect model inputs (e.g. climate forcing, grounding line position). The details of grounding line retreat and the rate at which information is transmitted upstream through the ice will strongly dictate the onshore thinning history, and, although we have attempted to reproduce a series of transient ice-sheet states, the temporal resolution of our time slice approach cannot reproduced the detailed history revealed by the cosmogenic data. We note that the thinning history in the North Masson Range (site 10), the closest site to the coast, is accurately reproduced by our model (Fig. 4a–d). Our model grounding line does not return to the coast until 5 ka BP in this region, and this results in a slower rate of thinning at this site.

Observations of ice thickness change within the Lambert Embayment (12–14) can only be reproduced if we assume that ice did not ground within the main trough north of ~72°20′S. In this

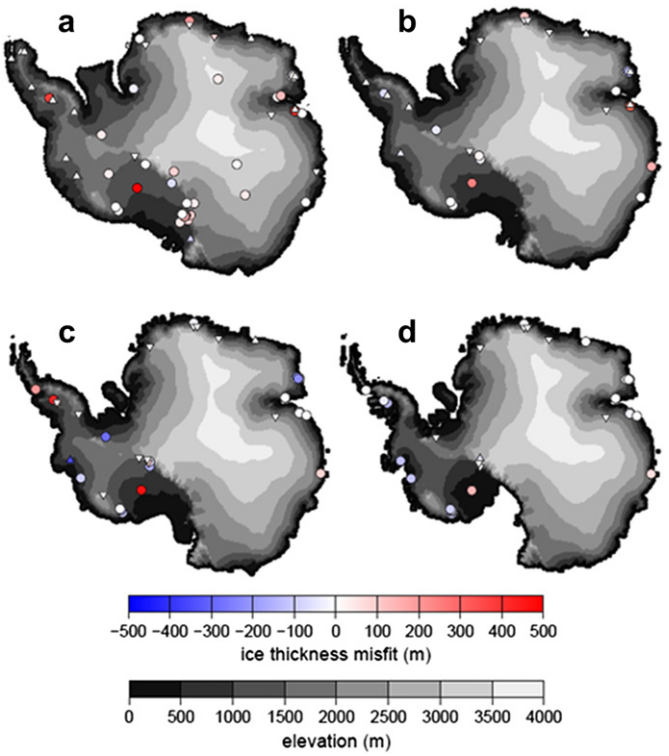

Fig. 5. Map view of ice thickness misfits at the data sites listed in Table 1. (a) 20 ka BP. (b) 15 ka BP. (c) 10 ka BP. (d) 5 ka BP. The greyscale represents the elevation of the ice-sheet reconstruction. Circles are absolute data sites, triangles are minimum limiting data, and inverted triangles are maximum limiting data. If the model reconstruction at a data site satisfies one of these limiting data then a zero misfit is assumed.

case, the observed change in ice thickness in the region of the Fisher Massif (12) at 20 ka BP (Mabin, 1992) is accurately reproduced by the model (Fig. 4a). However, non-zero ice-thickness change is still predicted at Radok Lake (13) and Amery Oasis (14) due to the low spatial resolution of our model (Fig. 4a). At all these sites, modelled ice thicknesses are back to present by 15 ka BP, in agreement with observations (Fig. 4b–d).

East of the Lambert Embayment, cosmogenic dating in the Grove Mountains (15) indicates that the ice-sheet surface has not been higher than present for at least 0.3 Ma (Lilly et al., 2010; Liu et al., 2010). If the Lambert Embayment is assumed to have contained grounded ice at the LGM, then this constraint is not satisfied, further justifying our choice of restricted grounding line advance. The data do not rule out the possibility of thinner ice in the Grove Mountains during the last glacial cycle, and in fact this situation is reproduced with a high degree of certainty by our model since a thinner-than-present ice sheet is predicted at 15 and 10 ka BP for the whole parameter space investigated (Fig. 4b/c).

The ice-free oases of the Stornes Peninsula (16), and the Larsemann (17) and Vestfold Hills (18) are small in area, and difficult to resolve on a 20 km resolution grid. The geological data are unable to place a maximum constraint on former ice-sheet thicknesses at the three sites, but our model thicknesses in the region of the Vestfold Hills lie within the range derived from the GIA modelling of relative sea-level data (Zwartz et al., 1998), indicating that our reconstruction should also fit these constraints. The post-20 ka BP grounding line history used in our reconstruction ensures that regional ice thicknesses are back to present by 10 ka BP, in agreement with observations (Fig. 4c/d). In contrast to the Stornes Peninsula and the Vestfold Hills, parts of the Larsemann Hills have been ice free throughout the LGM (Hodgson et al., 2001, 2005; Kiernan et al., 2009). This oasis is protected by the Dålk Glacier, which diverts ice around the ice-free region. The details of the local ice dynamics are not resolved in our model, therefore our model reconstruction indicates a thickening of the ice sheet in the grid cell containing the Larsemann Hills, and hence a large misfit to the data (site 17, Fig. 4a/b). Although we are unable to resolve the details of the ice-sheet history, there do exist relative sea-level data from this region (Verleyen et al., 2005) which will be sensitive to the regional loading history. These have been used to test the validity of the regional ice-sheet reconstruction (Whitehouse et al., in review).

The final oasis site within East Antarctica, the Bunger Hills, was ice free by ~20 ka BP (Gore et al., 2001). Anderson et al. (2002) place the LGM grounding line offshore in this location, but it is likely that this site is similar to the Larsemann Hills, in that the flow of the Scott and Remenchus Glaciers around the Bunger Hills has enabled this site to remain ice-free since the LGM. We follow the grounding line history of Anderson et al. (2002) and accept that our model reconstruction produces ice that is too thick at the Bunger Hills in the post-20 ka BP time slices (Fig. 4b–d, site 19). If the relative sea-level history of this region could be determined, it would be possible to place tighter constraints on the regional deglacial history.

6.1.2. Glaciological data

We use data from four East Antarctic ice cores to provide additional information on ice elevation changes across this region since the LGM. Three of the sites – Dome Fuji (20), Vostok (21), and Dome C (23) – are situated in the interior of the EAIS, and they form a ~2000 km-long transect across the centre of the continent (Fig. 5a). Flow modelling indicates that the surface of the ice was 100–200 m lower at all of these sites during the LGM (Jouzel et al., 1989; Parrenin et al., 2007) due to lower accumulation rates. The similarity of these observations adds weight to our assumption that the EAIS evolves in a uniform manner. Our model reproduces the observations to a high degree of accuracy (Fig. 4a), with misfits of $<$50 m at sites where the total ice thickness is $\geq$3000 m. These sites are strongly weighted in the misfit calculations due to the large area which each represents (see SOM), and the small residuals give us confidence that our model reconstruction, and hence volume calculation, is accurate over a large percentage of the EAIS. The fourth East Antarctic ice core that we use comes from the edge of the continent: At the Law Dome (22) the ice sheet is predicted to have been a few hundred metres thicker between 20 and 15 ka BP (Morgan et al., 1997; Delmotte et al., 1999), and once again this change in elevation is accurately reproduced by our model (Fig. 4a/b).

6.2. West Antarctica

6.2.1. Ross Sea

In West Antarctica we found it necessary to use the enhanced basal sliding parameter, B'_s, beneath the current and former ice streams of the Ross Sea (Fig. 2) in order to create a thinner ice sheet, and reproduce the ice-sheet profile that is preserved in the geological record along the margin of the Transantarctic Mountains. At the majority of sites only the maximum extent of ice during the last glacial cycle is recorded, although in several locations the initiation of thinning provides an important constraint upon the timing of grounding line retreat (Conway et al., 1999). Due to the complex topography of the region, and the complex geometry of the coastline, we check that the location of the nearest model grid point to each data site is physically realistic, i.e. that it lies onshore, or within the correct valley, and select the next closest grid point where necessary. Despite applying this check, we note that there are many sites along this coast which are poorly resolved by our model, making it difficult to compare observations and

predictions. In addition, short-period fluctuations of the numerical solution are a common feature in complex topography, and can lead to large differences in thinning histories in neighbouring grid cells. We attempt to reduce the influence of this effect by averaging over the last three time steps of each experiment, but the large range of ice thickness changes predicted for the Ross Sea sites (Fig. 4a, sites 24–42) indicates that the solutions are not very stable in this region. We find that our best-fit solution minimises the misfit in the Ross Sea when we use the thinnest ice-sheet reconstruction permitted by our parameter space, but the predicted change in ice thickness between 20 ka BP and the present day is still too large at nearly every Ross Sea site (Figs. 4a and 5a). Our modelled ice-sheet reconstruction in this region should therefore be regarded as a maximum.

Along the northern Ross Sea coast, the former thickness of the extended West Antarctic Ice Sheet (WAIS) is predominantly recorded at sites which are currently free of ice. Our model yields a good fit to the observations at the majority of these sites, which record ice thicknesses of 250–750 m during the LGM (Fig. 4a, sites 24–32). The misfit at Brown Peninsula (29, 31) is related to poor resolution of the local topography by the model. In contrast, observations of past ice thicknesses from glaciers which flow perpendicular to the Transantarctic Mountains indicate a gradient of thickening, with the greatest changes observed towards the grounding line and minimal changes observed at the edge of the East Antarctic Plateau. This is most clearly seen along the Hatherton and Beardmore Glaciers, where our model accurately reproduces the ~1000 m difference in ice thickness change between the upper and lower reaches of these glaciers at the LGM (Fig. 4a, sites 33–36). Further south, Todd et al. (2010) provide a high resolution thinning history for Reedy Glacier (37–41) using cosmogenic dating. We find that our model reconstruction thins a little too quickly near the grounding line between 20 ka BP and 10 ka BP (Fig. 4a–d, site 37), but that the total magnitude of the change is accurately reproduced. Higher up this glacier (sites 38–41), modelled changes in ice thicknesses are again slightly less than observed (Fig. 4b–d), but in general, our ice-sheet reconstruction along this glacier, and the nearby Ohio Glacier (42), agrees well with currently available observations.

6.2.2. Glaciological data

Two West Antarctic ice cores are used to constrain past ice elevations in the interior of Marie Byrd Land. The Byrd ice core (44) indicates that the ice sheet in this region was between 200 m lower and 300 m higher than present (Raynaud and Lebel, 1979; Jenssen, 1983; Grootes and Stuiver, 1986). Our model predicts an increase in ice elevation towards the upper limit of this range (Fig. 4a). At the location of the Siple Dome ice core (43), ice flow modelling has been used to deduce that the elevation of the ice sheet was 200–400 m higher at the LGM, with thinning to the present elevation complete by 10 ka BP (Waddington et al., 2005; Price et al., 2007). However, we note that Clark et al. (2009) use the observations of Brook et al. (2005) to suggest that ice could have been 500–600 m thicker than present at this site prior to 14.5 ka BP. All our ice-sheet reconstructions predict a considerably greater ice-elevation change at this site (Figs. 4a and 5a), with continuous thinning to the present day (Fig. 4b–d). We are unable to resolve this misfit by increasing the enhanced basal sliding parameter, B'_s, along the adjacent ice streams because we use a single value for all ice streams; if we increase this value such that $B'_s > 10$ then the ice-sheet reconstruction is too thin in other regions. One solution would be to invert for a spatially-variable basal sliding parameter. We do not adopt this approach here, and caution that our modelled ice-sheet reconstruction in the region of the Siple Coast should be regarded as a maximum reconstruction.

6.2.3. Marie Byrd Land and Amundsen Sea sector

East of the Ross Sea Embayment, our ice-sheet reconstruction once again lies within the bounds of the available observational constraints. Stone et al. (2003) use cosmogenic dating to determine the thinning history of the coastal Ford Ranges (45–49), and while our modelled ice thickness changes are towards the lower bound of the observed change between 20 ka BP and 10 ka BP (Fig. 4a–c), we accurately capture the final rate of deglaciation in this region (Fig. 4d). Temporal changes in ice thickness at Mount Waesche (50) are also accurately reproduced.

Within the Amundsen Sea Embayment our model highlights a disagreement between the marine and terrestrial records of deglaciation. The terrestrial record is not able to place a robust maximum constraint on the thickness of the WAIS at 20 ka BP because all the nunataks may have been covered by ice, but the thinning history can be deduced from measurements of cosmogenic isotopes (Johnson et al., 2008; Bentley et al., unpublished). We find close agreement between onshore observations and model predictions at 15 ka BP (Fig. 4b, site 52), but subsequent to this our model ice-sheet thins earlier than suggested by the onshore data (Fig. 4c, sites 51 and 52), driven by the large-scale retreat of the grounding line within the Amundsen Sea Embayment (Lowe and Anderson, 2002; Smith et al., 2011). Our time slice method is unable to resolve the detailed timing of retreat and thinning indicated by the data, but we highlight this as a key location for future research into the relationship between onshore and offshore ice-sheet processes.

6.2.4. Antarctic Peninsula

The largest uncertainties in our ice-sheet reconstruction are found along the Antarctic Peninsula (53–59). Our 20 km-resolution model is not able to resolve the underlying bedrock topography or the ice-sheet flow trajectories within this region, despite the use of a basal sliding mask to delineate faster flow along ice streams, with the result that our model produces a thick ice sheet along the Antarctic Peninsula for the 20 ka BP time slice. Many of the observational constraints from this region are minimum constraints, indicating that most nunataks were covered by ice at the LGM, but the observation at Ablation Point (55) (Bentley et al., 2006) provides a single 'ground-truth' measurement which indicates that our 20 ka BP reconstruction is likely several hundred metres too thick, at least in the region of Alexander Island. The thinning history in this region is surprisingly well-reproduced at 15 ka BP (Fig. 4b, sites 53–56), but the final rapid thinning which took place around 9.6 ka BP (Bentley et al., 2005) is not captured by our model (Fig. 5c), partly due to the spacing of our time slices, which means that we are unable to account for the rapid grounding line retreat between 10 ka BP and 9 ka BP (Bentley et al., 2005, 2011). Our model reconstructions predict thinner ice than present at 5 ka BP for several sites along George VI Sound (Fig. 4d, sites 53–55). This may be related to the decrease in the enhanced marine sliding parameter between the 5 ka BP time slice and the present day, which would cause ice velocities to decrease, and hence ice-sheet thickening, in regions which are dominated by flow along narrow ice streams but which experience little grounding line retreat during this period.

6.2.5. Weddell Sea

Palaeo ice-thickness constraints in the Weddell Sea sector (60–62) are very sparse. The thinning history of the Behrendt Mountains (60) (Bentley et al., 2006) is accurately reproduced by our model (Fig. 4a–c), indicating that our ice-sheet reconstruction in the southern Antarctic Peninsula may not be subject to the same limitations as in the northern Antarctic Peninsula. The magnitude of ice thickness change in the Ellsworth Mountains (61) (Bentley et al., 2010) between the LGM and present is also accurately

reproduced (Fig. 4a), but thinning takes place too early in our model (Figs. 4c and 5c), indicating that our deglacial grounding line positions are probably incorrect. At present there are no data available to constraint the extent or the retreat of the grounding line in this sector of Antarctica. In general, the predicted magnitude of thickening in the eastern Weddell Sea is less than that predicted for the western Weddell Sea. Our reconstruction underestimates previously-published magnitudes of ice-sheet thickening in the Shackleton Mountains (62) (Fogwill et al., 2004) (Fig. 4a, site 62), but overestimates more recent data that suggest much less LGM thickening in this region (Hein et al., 2011).

6.3. Summary of model fit to data

From Fig. 5 it is evident that our model fits the data well at locations throughout the continent, but there are large areas of Antarctica where our ice-sheet reconstruction is poorly constrained. Our best-fit 20 ka BP reconstruction either matches or slightly over-predicts the change in ice thickness between the present day and the LGM (Fig. 5a), and therefore this reconstruction provides an upper bound on the change in the volume of the AIS since the LGM. Our model achieves a high degree of fit to the available observations at 15 ka BP (Fig. 5b, anomalous sites are discussed above), however, at many sites our ice-sheet reconstruction thins too early in comparison to the data (blue dots, Fig. 5c), which seem to indicate that final deglaciation did not take place until after 10 ka BP at many locations. The sign of the misfit is reversed in the Antarctic Peninsula (red dots Fig. 5c), where our model predicts that final thinning took place more slowly than implied by the data. However, we note that the data used to constrain the 10 ka BP time slice in this region relate to the millennium immediately following 10 ka BP, during which rapid thinning is inferred to have taken place (Bentley et al., 2011), and we do not have tight constraints on the geometry of the ice-sheet immediately prior to this thinning event. By 5 ka BP, ice thickness change is complete at the majority of sites (Fig. 4d), and this is reproduced accurately by our model in East Antarctica (Fig. 5d). However, we find both positive and negative misfits in West Antarctica, indicating that our model is less accurate at capturing Late Holocene ice-sheet changes in this region.

7. Discussion

Our new AIS reconstruction is generated using a numerical ice-sheet model, and has been calibrated using observations of ice thickness change since the LGM at 62 sites around Antarctica. The degree of fit at 20 ka BP is good throughout East Antarctica, the Western Ross Sea, and Marie Byrd Land, but we find that our model predicts ice thickness changes which are too large along the Siple Coast and the Antarctic Peninsula, and the rate of deglaciation is not always accurately reproduced (Fig. 5). There are a few isolated sites in East Antarctica where our model does not accurately reproduce the observed ice thickness change (e.g. sites 4 and 17), but at these sites the misfit can be explained by the presence of local ice flow anomalies which are not reproduced within the resolution of our model.

7.1. Model limitations

Misfits between our model predictions and the field observations may be categorised as due to either model limitations or data limitations. Model limitations include (a) incomplete model physics resulting in the poor representation of physical processes such as ice streaming and water transport through the ice sheet, (b) a simplified treatment of spatial variations in basal sliding properties, (c) the use of a 20 km grid (limited by computing power), and (d) the use of a fixed grounding line, although we argue that the latter feature enables us to impose tight constraints upon the grounding line position where it is known. The spatial resolution of our model is the principal reason for large misfits in topographically complex areas because we are unable to resolve the details of ice flow in such areas, and the data sites themselves, often steep-sided nunataks, are not resolved within the topography. Other model limitations include the potentially incomplete sampling of the parameter space, and the use of incorrect boundary conditions. Uncertainty due to the latter is quantified in Fig. 6, where we plot the magnitude of the range of ice thicknesses generated when we vary the climate forcing, relative sea-level forcing, isostatic model, and geothermal heat flux distribution within reasonable bounds. A detailed breakdown of the contribution from each effect is discussed in the SOM.

7.2. Data limitations

Data limitations also impact the accuracy of our ice-sheet reconstruction. There are large spatial gaps, especially in East Antarctica and during the deglacial time slices (Fig. 5), and the proxy-based nature of the data, in particular the ice core data, makes it difficult to directly relate the observations to an absolute ice surface (Siddall et al., 2011). In addition, dating limitations in Antarctica (Bentley, 2010) mean that constraints are usually accompanied by large error bars. This uncertainty is not accounted for when we test our reconstruction against the field data because we assign each observation to a discrete time slice. In reality, these data relate to range of different periods, and the transient nature of the ice sheet during deglaciation means that our approach of modelling the ice sheet at discrete times makes it difficult for us to match predictions to observations. In some locations, such as the western Antarctic Peninsula (Bentley et al., 2011), deglaciation events took place very rapidly during short periods that fall between our time slices, whilst in other regions, such as East Antarctica, our grounding line mask indicates that deglaciation took place between 15 ka BP and 10 ka BP, but in reality the precise timing varied spatially around the coast. Neither of these subtleties

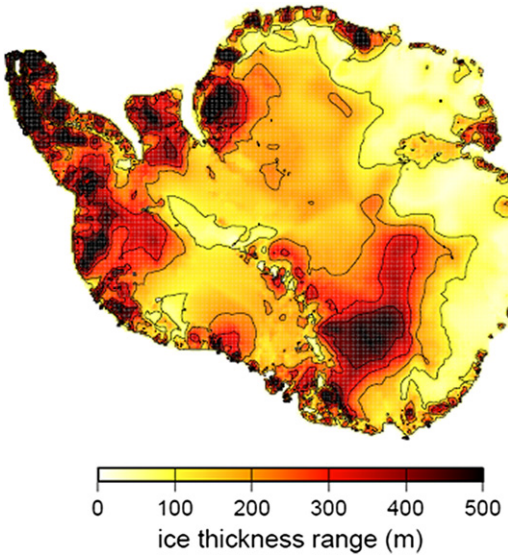

Fig. 6. The magnitude of the range of ice thicknesses generated when model parameters are varied through the full parameter space given in Table 2 (grounding line position and basal sliding parameters are held fixed at their optimum values – see text). This can be viewed as the uncertainty distribution for the 20 ka BP ice-sheet reconstruction.

is reproduced within our model, whereas the data will reflect these variations. As data density increases with ongoing marine and terrestrial glacial geological field programmes, future modelling may be able to user finer resolution time slices.

7.3. Sea-level equivalent

The equivalent eustatic contribution of our ice-sheet reconstruction is determined by calculating the change in the thickness of ice above buoyancy between each palaeo time slice and the present day, converting this ice volume to a water volume, and dividing by the area of the present-day ocean. We compare each palaeo reconstruction to our present-day *model* solution rather than observed present-day ice thicknesses since we are interested in the change in ice loading during deglaciation, as predicted by our model. The suite of model reconstructions defined by the parameter space of Table 2 (holding grounding line positions and basal sliding parameters at their optimum values) contributes 9 ± 1.5 m eustatic sea level to the global ocean between 20 ka BP and the present day, and our best-fit reconstruction contributes ~8 m eustatic sea level during this period (Fig. 7a). These values are much smaller than many previous estimates (Bentley, 1999, 2010), but are in reasonable agreement with the reconstruction of Ivins and James (2005). Given the observational constraints on the thickness of the ice sheet at the LGM, and the consistency of our solution in unconstrained regions (due to the use of a numerical ice-sheet model) we conclude that many earlier estimates are too high.

At many sites we have used the maximum observed change in ice-sheet thickness during the last glacial cycle as a proxy for the change in ice thickness between 20 ka BP and the present day. Such field observations relate to the local LGM in each region, but this is unlikely to have been synchronous throughout Antarctica. In several regions, such as Dronning Maud Land and the Eastern Ross Sea, deglaciation had already begun by 20 ka BP (Anderson et al., 2002; Mosola and Anderson, 2006), whilst in others, such as the Western Ross Sea, marine data imply that the maximum ice-sheet extent was not reached until after 20 ka BP (Licht and Andrews, 2002). There is ambiguity over the timing of the volumetric LGM in Antarctica (Bentley, 1999; Clark et al., 2009), which has implications for the interpretation of far-field relative sea-level observations. There are also very few constraints on the duration of the local LGM around Antarctica, and this will have a direct bearing upon the magnitude of deformation, and subsequent rate of rebound, of the solid earth.

We are unable to resolve the detailed timing of the eustatic contribution due to the time slice method that we have adopted, but it is clear that the excess volume of ice available around 14.5 ka BP was insufficient to provide the dominant source for meltwater pulse 1A (Clark et al., 1996, 2002; Weaver et al., 2003; Bassett et al., 2007). Our model predicts a small eustatic contribution of ~2 m during the Late Holocene, in agreement with the predictions of Lambeck (2002), who used far-field observations to determine the magnitude of eustatic sea-level change since the final deglaciation of the northern hemisphere ice sheets. At present only limited work has been carried out to determine the source of this Late Holocene contribution (Stocchi et al., 2009).

The eustatic volume of our 20 ka BP ice-sheet reconstructions vary by ~3 m (Fig. 7a) depending upon the choice of model parameters (Table 2). This range is due to uncertainty in modelled ice thickness changes, particularly in West Antarctica (Fig. 6). Consideration of the range at each data site (Fig. 4a) indicates that many of the solutions over-predict the geological observations, and that even our best-fit solution should be regarded as an upper bound on the change in Antarctic ice volume between 20 ka BP and the present day. In order to provide a realistic history of ice loading for the purposes of GIA modelling our reconstruction should be further tuned using relative sea-level data and bedrock velocities, such as from GPS data.

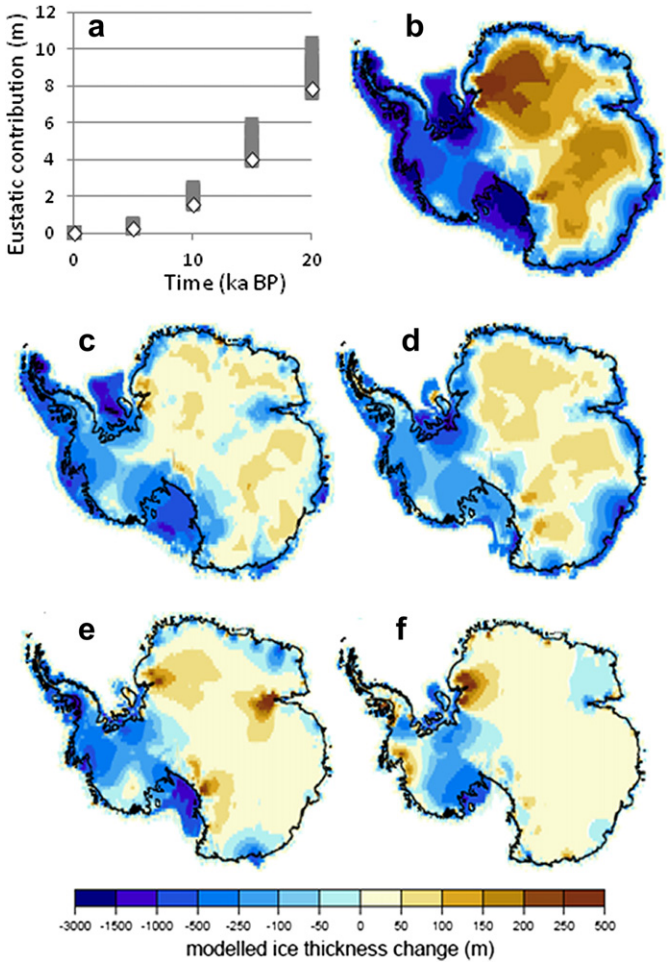

Fig. 7. Modelled ice volume change over last 20 ka. (a) Excess ice volume through time compared to our present-day ice-sheet reconstruction, in metres of equivalent eustatic sea level. The range of values generated by sampling the parameter space in Table 2 is shown by the grey bar; the values for our best-fit model are shown as white diamonds. We also plot model change in ice thickness between (b) 20 ka BP and our present-day reconstruction, (c) 20 ka BP and 15 ka BP, (d) 15 ka BP and 10 ka BP, (e) 10 ka BP and 5 ka BP, and (f) 5 ka BP and our present-day reconstruction. Blue colours represent ice thinning through time, brown colours represent ice thickening. Note the different scales for positive and negative changes. (For interpretation of the references to colour in this figure legend, the reader is referred to the web version of this article.)

7.4. Ice-thickness change

The distribution of predicted ice thickness change (proportional to mass change) since 20 ka BP is shown in Fig. 7b–f, where the dark blue areas across West Antarctica and the Antarctic Peninsula indicate that these are the dominant sources of meltwater in our model. The meltwater contribution from East Antarctica is sourced from the margins of the ice sheet (Fig. 7b), due to grounding line retreat. In the interior of East Antarctica, our model predicts that ice thicknesses have increased since the LGM, in agreement with ice core measurements, due to the increase in accumulation rates during this period. Our model predicts continued ice mass loss between 5 ka BP and the present day (Fig. 7f) due to continued grounding line retreat in the Ross and Weddell Seas. The recent (millennial-scale) grounding line history is poorly constrained in these regions, and field observations indicate that there is ongoing

retreat in some areas (Stone et al., 2003), whilst in others ice flow has stagnated during the last few millennia (King, 2011). A higher resolution modelling approach is required in order to reproduce the spatially-variable changes which have taken place throughout West Antarctica during the last few thousand years, and to understand the dynamic relationship between climatic changes and ice-sheet changes during this period.

7.5. Comparison to previous work

Our total Antarctic eustatic sea-level contribution of 9 ± 1.5 m between 20 ka BP and the present day is similar to values obtained by the previous numerical modelling studies of Ritz et al. (5.9 m; 2001), Philippon et al. (9.5–17.5 m; 2006) and Pollard and DeConto (~12.5 m in their nominal run; 2009). The distribution of present-day ice thickness misfits (Fig. 2) and LGM ice elevations (Fig. 5a) derived within our model is also very similar to the results of two of these studies (Ritz et al., 2001; Pollard and DeConto, 2009), indicating that these independent models seem to have captured the physics of ice flow in a similar fashion. All three of the studies mentioned above recognise the importance of correctly defining basal sliding parameters in order to reproduce ice streams and the concave ice-sheet profile observed in marine-grounded areas, in agreement with our findings.

There are small differences in the LGM reconstructions: Pollard and DeConto (2009) have a more extensive grounding line in the Amery Basin compared to our model, and their pattern of grounding line retreat in the Ross Sea is slightly different. Our pattern of grounding line maximum extent and retreat in the Weddell Sea is very different to both the Ritz et al. (2001) and Pollard and DeConto (2009) studies due to our assumption that ice was not grounded along the deep marine troughs of this region. This has an impact upon the pattern of LGM ice surface elevation in the Weddell Sea embayment, and therefore affects the dynamics of the ice-sheet reconstructions in this region. We also note that our surface elevation contours at all time slices are indented across the Recovery Basin, unlike those in the Ritz et al. (2001) and Pollard and DeConto (2009) reconstructions. The difference is likely due to our use of updated bedrock topography in this region (Le Brocq et al., 2008) which more accurately reproduces the present-day profile of the ice sheet.

8. Conclusions

In summary, the new deglacial model for Antarctica presented in this paper – derived from numerical modelling and tightly constrained by geological data – provides an updated estimate for the LGM ice-sheet volume that is lower than many previous estimates, and that can be used to constrain the Holocene global meltwater budget. The reconstructed pattern of ice unloading can also serve as an input for glacial isostatic models: The new ice-loading history will be used to calculate time-dependent relative sea-level change and present-day uplift rates throughout Antarctica, and comparisons to data will permit us to test the validity of our deglacial reconstruction and place constraints on the rheological properties of the solid Earth beneath Antarctica.

This study highlights that there is a pressing need for more information on past grounding-line positions, especially following the LGM, and for further investigations of key areas where data are still sparse, even by Antarctic standards. These include the East Antarctic margin, Weddell Sea, and key parts of the West Antarctic Ice Sheet including Marie Byrd Land and Amundsen Sea regions. The current lack of data makes it difficult to test our ice-sheet reconstruction in these regions, and alternative methods of reconstructing ice-sheet changes, such as the interpretation of internal ice-sheet layering, might be further explored.

Acknowledgements

We thank numerous colleagues with whom we have discussed former ice extent and thickness data. Stewart Jamieson, Stephen Livingstone, Matt King and Glenn Milne all provided helpful discussion on specific modelling or data issues. We also thank Erik Ivins and an anonymous reviewer for providing useful comments on the manuscript. The work was carried out under NERC Grant NE/E004806.

Appendix. Supplementary material

Supplementary material associated with this article can be found, in the online version, at doi:10.1016/j.quascirev.2011.11.016.

References

Ackert, R.P., Barclay, D.J., Borns, H.W., Calkin, P.E., Kurz, M.D., Fastook, J.L., Steig, E.J., 1999. Measurements of past ice sheet elevations in interior West Antarctica. Science 286, 276–280.
Ackert, R.P., Mukhopadhyay, S., Parizek, B.R., Borns, H.W., 2007. Ice elevation near the West Antarctic Ice Sheet divide during the Last Glaciation. Geophysical Research Letters 34.
Adamson, D.A., Mabin, M.C.G., Luly, J.G., 1997. Holocene isostasy and late Cenozoic development of landforms including Beaver and Radok Lake basins in the Amery Oasis, Prince Charles Mountains, Antarctica. Antarctic Science 9, 299–306.
Adamson, D.A., Colhoun, E.A., 1992. Late quaternary glaciation and deglaciation of the Bunger Hills, Antarctica. Antarctic Science 4, 435–446.
Anderson, J.B., Shipp, S.S., Lowe, A.L., Wellner, J.S., Mosola, A.B., 2002. The Antarctic Ice Sheet during the Last Glacial Maximum and its subsequent retreat history: a review. Quaternary Science Reviews 21, 49–70.
Anderson, B.M., Hindmarsh, R.C.A., Lawson, W.J., 2004. A modelling study of the response of Hatherton Glacier to Ross Ice Sheet grounding line retreat. Global and Planetary Change 42, 143–153.
Arthern, R.J., Winebrenner, D.P., Vaughan, D.G., 2006. Antarctic snow accumulation mapped using polarization of 4.3-cm wavelength microwave emission. Journal of Geophysical Research-Atmospheres 111.
Bamber, J.L., Gomez-Dans, J.L., Griggs, J.A., 2009. A new 1 km digital elevation model of the Antarctic derived from combined satellite radar and laser data – part 1: data and methods. Cryosphere 3, 101–111.
Baroni, C., Orombelli, G., 1987. Glacial geology and geomorphology of Terra Nova Bay. Memorie Società Geologica Italiana 33, 171–193.
Bassett, S.E., Milne, G.A., Bentley, M.J., Huybrechts, P., 2007. Modelling Antarctic sea-level data to explore the possibility of a dominant Antarctic contribution to meltwater pulse IA. Quaternary Science Reviews 26, 2113–2127.
Bentley, M.J., 1999. Volume of Antarctic ice at the Last Glacial Maximum, and its impact on global sea level change. Quaternary Science Reviews 18, 1569–1595.
Bentley, M.J., 2010. The Antarctic palaeo record and its role in improving predictions of future Antarctic Ice Sheet change. Journal of Quaternary Science 25, 5–18.
Bentley, M.J., Fogwill, C.J., Kubik, P.W., Sugden, D.E., 2006. Geomorphological evidence and cosmogenic Be-10/Al-26 exposure ages for the Last Glacial Maximum and deglaciation of the Antarctic Peninsula Ice Sheet. Geological Society of America Bulletin 118, 1149–1159.
Bentley, M.J., Fogwill, C.J., Le Brocq, A.M., Hubbard, A.L., Sugden, D.E., Dunai, T.J., Freeman, S.P.H.T., 2010. Deglacial history of the west Antarctic Ice Sheet in the Weddell Sea embayment: constraints on past ice volume change. Geology 38, 411–414.
Bentley, M.J., Hodgson, D.A., Smith, J.A., Cox, N.J., 2005. Relative sea level curves for the South Shetland Islands and Marguerite Bay, Antarctic Peninsula. Quaternary Science Reviews 24, 1203–1216.
Bentley, M.J., Johnson, J.S., Hodgson, D.A., Dunai, T., Freeman, S.P.H.T., Ó Cofaigh, C., 2011. Rapid deglaciation of Marguerite Bay, western Antarctic Peninsula in the early Holocene. Quaternary Science Reviews 30, 3338–3349.
Blunier, T., Schwander, J., Chappellaz, J., Parrenin, F., Barnola, J.M., 2004. What was the surface temperature in central Antarctica during the Last Glacial Maximum? Earth and Planetary Science Letters 218, 379–388.
Bockheim, J.G., Wilson, S.C., Denton, G.H., Andersen, B.G., Stuiver, M., 1989. Late Quaternary ice-surface fluctuations of Hatherton Glacier, Transantarctic Mountains. Quaternary Research 31, 229–254.
Brook, E.J., White, J.W.C., Schilla, A.S.M., Bender, M.L., Barnett, B., Severinghaus, J.P., Taylor, K.C., Alley, R.B., Steig, E.J., 2005. Timing of millennial-scale climate change at Siple Dome, West Antarctica, during the last glacial period. Quaternary Science Reviews 24, 1333–1343.
Budd, W.F., Jenssen, D., Smith, I.N., 1984. A 3-dimensional time-dependent model of the West Antarctic Ice-Sheet. Annals of Glaciology 5, 29–36.
Burgess, J.S., Spate, A.P., Shevlin, J., 1994. The onset of deglaciation in the Larsemann Hills, Eastern Antarctica. Antarctic Science 6, 491–495.
Canals, M., Urgeles, R., Calafat, A.M., 2000. Deep sea-floor evidence of past ice streams off the Antarctic Peninsula. Geology 28, 31–34.

Chen, J.L., Wilson, C.R., Blankenship, D., Tapley, B.D., 2009. Accelerated Antarctic ice loss from satellite gravity measurements. Nature Geoscience 2, 859–862.
Chen, J.L., Wilson, C.R., Blankenship, D.D., Tapley, B.D., 2006. Antarctic mass rates from GRACE. Geophysical Research Letters 33.
Chen, J.L., Wilson, C.R., Tapley, B.D., Blankenship, D., Young, D., 2008. Antarctic regional ice loss rates from GRACE. Earth and Planetary Science Letters 266, 140–148.
Clark, P.U., Alley, R.B., Keigwin, L.D., Licciardi, J.M., Johnsen, S.J., Wang, H.X., 1996. Origin of the first global meltwater pulse following the Last Glacial Maximum. Paleoceanography 11, 563–577.
Clark, P.U., Dyke, A.S., Shakun, J.D., Carlson, A.E., Clark, J., Wohlfarth, B., Mitrovica, J.X., Hostetler, S.W., McCabe, A.M., 2009. The Last Glacial Maximum. Science 325, 710–714.
Clark, P.U., Mitrovica, J.X., Milne, G.A., Tamisiea, M.E., 2002. Sea-level fingerprinting as a direct test for the source of global meltwater pulse IA. Science 295, 2438–2441.
Comiso, J.C., 2000. Variability and trends in Antarctic surface temperatures from in situ and satellite infrared measurements. Journal of Climate 13, 1674–1696.
Conway, H., Hall, B.L., Denton, G.H., Gades, A.M., Waddington, E.D., 1999. Past and future grounding-line retreat of the West Antarctic Ice Sheet. Science 286, 280–283.
Delmotte, M., Raynaud, D., Morgan, V., Jouzel, J., 1999. Climatic and glaciological information inferred from air-content measurements of a Law Dome (East Antarctica) ice core. Journal of Glaciology 45, 255–263.
Denton, G.H., Hughes, T.J., 2002. Reconstructing the Antarctic Ice Sheet at the Last Glacial Maximum. Quaternary Science Reviews 21, 193–202.
Denton, G.H., Marchant, D.R., 2000. The geologic basis for a reconstruction of a grounded ice sheet in McMurdo Sound, Antarctica, at the last glacial maximum. Geografiska Annaler Series A, Physical Geography 82, 167–211.
Denton, G.H., Bockheim, J.G., Wilson, S.C., Leide, J.E., Andersen, B.G., 1989. Late quaternary ice-surface fluctuations of Beardmore Glacier, Transantarctic Mountains. Quaternary Research 31, 183–209.
Dyke, A.S., Prest, V.K., 1987. Late Wisconsinian and Holocene history of the Laurentide Ice Sheet. Geographie physique et Quaternaire 41, 237–263.
Fabel, D., Stone, J., Fiefield, L.K., Cresswell, R.G., 1997. Deglaciation of the Vestfold Hills, East Antarctica: preliminary evidence from exposure dating of three subglacial erratics. In: Ricci, C.A. (Ed.), The Antarctic Region: Geological Evolution and Processes. Terra Antarctica Publication, Siena, pp. 829–834.
Fink, D., McKelvey, B., Hambrey, M.J., Fabel, D., Brown, R., 2006. Pleistocene deglaciation chronology of the Amery Oasis and Radok Lake, northern Prince Charles Mountains, Antarctica. Earth and Planetary Science Letters 243, 229–243.
Fogwill, C.J., Bentley, M.J., Sugden, D.E., Kerr, A.R., Kubik, P.W., 2004. Cosmogenic nuclides Be-10 and Al-26 imply limited Antarctic Ice Sheet thickening and low erosion in the Shackleton Range for >1 m.y. Geology 32, 265–268.
Fox Maule, C., Purucker, M.E., Olsen, N., Mosegaard, K., 2005. Heat flux anomalies in Antarctica revealed by satellite magnetic data. Science 309, 464–467.
Gore, D.B., Rhodes, E.J., Augustinus, P.C., Leishman, M.R., Colhoun, E.A., Rees-Jones, J., 2001. Bunger Hills, East Antarctica: ice free at the Last Glacial Maximum. Geology 29, 1103–1106.
Grootes, P.M., Stuiver, M., 1986. Ross ice shelf Oxygen isotopes and West Antarctic climate history. Quaternary Research 26, 49–67.
Gyllencreutz, G., Mangerud, J., Svendsen, J.-I., Lohne, Ø., 2007. DATED – A GIS-based reconstruction and dating database of the Eurasian deglaciation. In: Johansson, P., Sarala, P. (Eds.), Applied Quaternary Research in the Central Part of Glaciated Terrain. Geological Survey of Finland, pp. 113–120.
Hall, B.L., 2009. Holocene glacial history of Antarctica and the sub-Antarctic islands. Quaternary Science Reviews 28, 2213–2230.
Hall, B.L., Denton, G.H., 1999. New relative sea-level curves for the southern Scott Coast, Antarctica: evidence for Holocene deglaciation of the western Ross Sea. Journal of Quaternary Science 14, 641.
Hall, B.L., Denton, G.H., 2000. Extent and chronology of the Ross Sea ice sheet and the Wilson Piedmont glacier along the Scott Coast at and since the last glacial maximum. Geografiska Annaler Series A, Physical Geography 82, 337–363.
Hall, B.L., Denton, G.H., Overturf, B., 2001. Glacial Lake Wright, a high-level Antarctic lake during the LGM and early Holocene. Antarctic Science 13, 53–60.
Hall, B.L., Henderson, G.M., Baroni, C., Kellogg, T.B., 2010. Constant Holocene Southern-Ocean (14)C reservoir ages and ice-shelf flow rates. Earth and Planetary Science Letters 296, 115–123.
Haran, T., Bohlander, J., Scambos, T., Painter, T., Fahnestock, M., 2005 (updated 2006). MODIS Mosaic of Antarctica (MOA) Image Map. National Snow and Ice Data Center, Digital Media, Boulder, Colorado, USA.
Hättestrand, C., Johansen, N., 2005. Supraglacial moraines in Scharffenbergbotnen, Heimefrontfjella, Dronning Maud Land, Antarctica – significance for reconstructing former blue ice areas. Antarctic Science 17, 225–236.
Hayashi, M., Yoshida, Y., 1994. Holocene raised beaches in the Lützow-Holm Bay region, East Antarctica. Memoirs of National Institute of Polar Research Special Issue 50, 49–84.
Hein, A.S., Fogwill, C.J., Sugden, D.E., Xu, S., 2011. Glacial/interglacial ice-stream stability in the Weddell Sea embayment, Antarctica. Earth and Planetary Science Letters 307, 211–221.
Heroy, D.C., Anderson, J.B., 2005. Ice-sheet extent of the Antarctic Peninsula region during the Last Glacial Maximum (LGM) – Insights from glacial geomorphology. Geological Society of America Bulletin 117, 1497–1512.
Heroy, D.C., Anderson, J.B., 2007. Radiocarbon constraints on Antarctic Peninsula Ice Sheet retreat following the Last Glacial Maximum (LGM). Quaternary Science Reviews 26, 3286–3297.
Hiller, A., Wand, U., Kampf, H., Stackebrandt, W., 1988. Occupation of the Antarctic continent by petrels during the past 35000 years – inferences from a C-14 study of stomach oil deposits. Polar Biology 9, 69–77.
Hiller, A., Hermichen, W.D., Wand, U., 1995. Radiocarbon-dated subfossil stomach oil deposits from petrel nesting sites: Novel paleoenvironmental records from continental Antarctica. Radiocarbon 37, 171–180.
Hodgson, D.A., Noon, P.E., Vyverman, W., Bryant, C.L., Gore, D.B., Appleby, P., Gilmour, M., Verleyen, E., Sabbe, K., Jones, V.J., Ellis-Evans, J.C., Wood, P.B., 2001. Were the Larsemann Hills ice-free through the Last Glacial Maximum? Antarctic Science 13, 440–454.
Hodgson, D.A., Verleyen, E., Sabbe, K., Squier, A.H., Keely, B.J., Leng, M.J., Saunders, K.M., Vyverman, W., 2005. Late Quaternary climate-driven environmental change in the Larsemann Hills, East Antarctica, multi-proxy evidence from a lake sediment core. Quaternary Research 64, 83–99.
Hodgson, D.A., Roberts, S.J., Bentley, M.J., Smith, J.A., Johnson, J.S., Verleyen, E., Vyverman, W., Hodson, A.J., Leng, M.J., Cziferszky, A., Fox, A.J., Sanderson, D.C.W., 2009. Exploring former subglacial Hodgson Lake, Antarctica Paper I: site description, geomorphology and limnology. Quaternary Science Reviews 28, 2295–2309.
Huybrechts, P., 2002. Sea-level changes at the LGM from ice-dynamic reconstructions of the Greenland and Antarctic Ice Sheets during the glacial cycles. Quaternary Science Reviews 21, 203–231.
Ivins, E.R., James, T.S., 2005. Antarctic glacial isostatic adjustment: a new assessment. Antarctic Science 17, 541–553.
Jenssen, D., 1983. Elevation and climatic change from total gas content and stable isotope measurements. In: Robin, G.d.Q. (Ed.), The Climatic Record in Polar Ice Sheets. Cambridge University Press, Cambridge, pp. 138–144.
Jonsson, S., 1988. Observations on the physical geography and glacial history of the Vestfjella nunataks in western Dronning Maud Land, Antarctica, Forskningsrapport. Naturgeografiska Institutionen, Stockholms Universitet, 57 pp.
Johnson, J.S., Bentley, M.J., Gohl, K., 2008. First exposure ages from the Amundsen Sea embayment, West Antarctica: the late Quaternary context for recent thinning of Pine Island, Smith, and Pope Glaciers. Geology 36, 223–226.
Johnson, J.S., Bentley, M.J., Roberts, S.J., Binnie, S.A., Freeman, S.P., 2011. Holocene deglacial history of the north east Antarctic Peninsula – a review and new chronological constraints. Quaternary Science Reviews 30, 3791–3802.
Joughin, I., Tulaczyk, S., 2002. Positive mass balance of the Ross ice streams, West Antarctica. Science 295, 476–480.
Jouzel, J., Masson-Delmotte, V., Cattani, O., Dreyfus, G., Falourd, S., Hoffmann, G., Minster, B., Nouet, J., Barnola, J.M., Chappellaz, J., Fischer, H., Gallet, J.C., Johnsen, S., Leuenberger, M., Loulergue, L., Luethi, D., Oerter, H., Parrenin, F., Raisbeck, G., Raynaud, D., Schilt, A., Schwander, J., Selmo, E., Souchez, R., Spahni, R., Stauffer, B., Steffensen, J.P., Stenni, B., Stocker, T.F., Tison, J.L., Werner, M., Wolff, E.W., 2007. Orbital and millennial Antarctic climate variability over the past 800,000 years. Science 317, 793–796.
Jouzel, J., Raisbeck, G., Benoist, J.P., Yiou, F., Lorius, C., Raynaud, D., Petit, J.R., Barkov, N.I., Korotkevitch, Y.S., Kotlyakov, V.M., 1989. A comparison of deep Antarctic ice cores and their implications for climate between 65,000 and 15,000 years ago. Quaternary Research 31, 135–150.
Jouzel, J., Vimeux, F., Caillon, N., Delaygue, G., Hoffmann, G., Masson-Delmotte, V., Parrenin, F., 2003. Magnitude of isotope/temperature scaling for interpretation of central Antarctic ice cores. Journal of Geophysical Research-Atmospheres 108.
Kerr, A., Hermichen, W.D., 1999. Glacial modification of the Shackleton Range, Antarctica. Terra Antarctica 6, 353–360.
Kiernan, K., Gore, D.B., Fink, D., White, D.A., McConnell, A., Sigurdsson, I.A., 2009. Deglaciation and weathering of Larsemann Hills, East Antarctica. Antarctic Science 21, 373–382.
King, E.C., 2011. Ice stream or not? radio-echo sounding of Carlson Inlet, West Antarctica. The Cryosphere 5, 907–916.
Krause, W.E., Krbetschek, M.R., Stolz, W., 1997. Dating of Quaternary lake sediments from the Schirmacher oasis (east Antarctica) by infrared stimulated luminescence (IRSL) detected at the wavelength of 560 nm. Quaternary Science Reviews 16, 387–392.
Krinner, G., Raynaud, D., Doutriaux, C., Dang, H., 2000. Simulations of the Last Glacial Maximum ice sheet surface climate: implications for the interpretation of ice core air content. Journal of Geophysical Research-Atmospheres 105, 2059–2070.
Lambeck, K., 2002. Sea-level change from mid-Holocene to recent time: an Australian example with global implications. In: Mitrovica, J.X., Vermeersen, L.A. (Eds.), Ice Sheets, Sea Level and the Dynamic Earth. American Geophysical Union, Washington, pp. 33–50.
Le Brocq, A.M., Bentley, M.J., Hubbard, A., Fogwill, C.J., Sugden, D.E., Whitehouse, P.L., 2011. Reconstructing the Last Glacial Maximum ice sheet in the Weddell Sea embayment, Antarctica, using numerical modelling constrained by field evidence. Quaternary Science Reviews 30, 2422–2432.
Le Brocq, A.M., Hubbard, A., Bentley, M.J., Bamber, J.L., 2008. Subglacial topography inferred from ice surface terrain analysis reveals a large un-surveyed basin below sea level in East Antarctica. Geophysical Research Letters 35.
Le Brocq, A.M., Payne, A.J., Vieli, A., 2010. An improved Antarctic dataset for high resolution numerical ice sheet models (ALBMAP v1). Earth System Science Data 2, 247–260.
Le Meur, E., Huybrechts, P., 1996. A comparison of different ways of dealing with isostasy: examples from modelling the Antarctic Ice Sheet during the last glacial cycle. Annals of Glaciology 23, 309–317.
Licht, K.J., Andrews, J.T., 2002. The C-14 record of Late Pleistocene ice advance and retreat in the central Ross Sea, Antarctica. Arctic Antarctic and Alpine Research 34, 324–333.

Lilly, K., Fink, D., Fabel, D., Lambeck, K., 2010. Pleistocene dynamics of the interior East Antarctic Ice Sheet. Geology 38, 703–706.
Lintinen, P., Nenonen, J., 1997. Glacial history of the Vestfjella and Heimefrontfjella nunatak ranges in western Dronning Maud Land, Antarctica. In: Ricci, C.A. (Ed.), The Antarctic Region: Geological Evolution and Processes. Terra Antarctica Publications, Siena, pp. 845–852.
Liu, X., Huang, F., Kong, P., Fang, A., Li, X., Ju, Y., 2010. History of ice sheet elevation in East Antarctica: Paleoclimatic implications. Earth and Planetary Science Letters 290, 281–288.
Lorius, C., Raynaud, D., Petit, J.R., Jouzel, J., Merlivat, L., 1984. Lateglacial maximum-Holocene atmospheric and ice-thickness changes from Antarctic ice-core studies. Annals of Glaciology 5, 88–94.
Lowe, A.L., Anderson, J.B., 2002. Reconstruction of the West Antarctic Ice Sheet in Pine Island Bay during the Last Glacial Maximum and its subsequent retreat history. Quaternary Science Reviews 21, 1879–1897.
Mabin, M.C.G., 1991. The glacial history of the Lambert Glacier – Prince Charles Mountains area and comparisons with the record from the Transantarctic Mountains. In: Gillieson, D., Fitzsimons, S. (Eds.), Quaternary Research in Australian Antarctica. Department of Geography and Oceanography, Australian Defence Force Academy, Canberra, pp. 15–23.
Mabin, M.C.G., 1992. Late Quaternary ice-surface fluctuations of the Lambert Glacier. In: Yoshida, Y. (Ed.), Recent Progress in Antarctic Earth Science. Terrapub, Tokyo, pp. 683–687.
Mackintosh, A., Golledge, N., Domack, E., Dunbar, R., Leventer, A., White, D., Pollard, D., DeConto, R., Fink, D., Zwartz, D., Gore, D., Lavoie, C., 2011. Retreat of the East Antarctic Ice Sheet during the last glacial termination. Nature Geoscience 4, 195–202.
Mackintosh, A., White, D., Fink, D., Gore, D.B., Pickard, J., Fanning, P.C., 2007. Exposure ages from mountain dipsticks in Mac. Robertson Land, East Antarctica, indicate little change in ice-sheet thickness since the Last Glacial Maximum. Geology 35, 551–554.
Magand, O., Frezzotti, M., Pourchet, M., Stenni, B., Genoni, L., Fily, M., 2004. Climate variability along latitudinal and longitudinal transects in east Antarctica. Annals of Glaciology 39, 351–358.
Martinerie, P., Lipenkov, V.Y., Raynaud, D., Chappellaz, J., Barkov, N.I., Lorius, C., 1994. Air content paleo record in the Vostok ice core (Antarctica) – a mixed record of climatic and glaciological parameters. Journal of Geophysical Research-Atmospheres 99, 10565–10576.
Mitrovica, J.X., Milne, G.A., 2003. On post-glacial sea level: I. General theory. Geophysical Journal International 154, 253–267.
Mitrovica, J.X., Wahr, J., Matsuyama, I., Paulson, A., 2005. The rotational stability of an ice-age earth. Geophysical Journal International 161, 491–506.
Miura, H., Moriwaki, K., Maemoku, H., Hirakawa, K., 1998. Fluctuations of the East Antarctic ice-sheet margin since the last glaciation from the stratigraphy of raised beach deposits along the Sôya Coast. Annals of Glaciology 27, 297–301.
Morelli, A., Danesi, S., 2004. Seismological imaging of the Antarctic continental lithosphere: a review. Global and Planetary Change 42, 155–165.
Moriwaki, K., Hirakawa, K., Matsuoka, N., 1991. Weathering stage of till and glacial history of the Central Sør Rondane Mountains, East Antarctica. Proceedings of the NIPR Symposium on Antarctic Geosciences 5, 99–111.
Moriwaki, K., Hirakawa, K., Hayashi, M., Iwata, S., 1992. Late Cenozoic glacial history in the Sør-Rondane Mountains, East Antarctica. In: Yoshida, Y. (Ed.), Recent Progress in Antarctic Earth Science. Terra Scientific Publishing Company, Tokyo, pp. 661–667.
Morgan, V.I., Wookey, C.W., Li, J., van Ommen, T.D., Skinner, W., Fitzpatrick, M.F., 1997. Site information and initial results from deep ice drilling on Law dome, Antarctica. Journal of Glaciology 43, 3–10.
Mosola, A.B., Anderson, J.B., 2006. Expansion and rapid retreat of the West Antarctic Ice Sheet in eastern Ross Sea: possible consequence of over-extended ice streams? Quaternary Science Reviews 25, 2177–2196.
Muszynski, I., Birchfield, G.E., 1985. The dependence of Antarctic accumulation rates on surface-temperature and elevation. Tellus Series A-Dynamic Meteorology and Oceanography 37, 204–208.
Nakada, M., Lambeck, K., 1988. The melting history of the Late Pleistocene Antarctic Ice-Sheet. Nature 333, 36–40.
Parrenin, F., Dreyfus, G., Durand, G., Fujita, S., Gagliardini, O., Gillet, F., Jouzel, J., Kawamura, K., Lhomme, N., Masson-Delmotte, V., Ritz, C., Schwander, J., Shoji, H., Uemura, R., Watanabe, O., Yoshida, N., 2007. 1-D-ice flow modelling at EPICA Dome C and Dome Fuji, East Antarctica. Climate of the Past 3, 243–259.
Parrenin, F., Remy, F., Ritz, C., Siegert, M.J., Jouzel, J., 2004. New modeling of the Vostok ice flow line and implication for the glaciological chronology of the Vostok ice core. Journal of Geophysical Research-Atmospheres 109.
Peltier, W.R., 2004. Global glacial isostasy and the surface of the ice-age earth: the ICE-5G (VM2) model and GRACE. Annual Review of Earth and Planetary Sciences 32, 111–149.
Petit, J.R., Jouzel, J., Raynaud, D., Barkov, N.I., Barnola, J.M., Basile, I., Bender, M., Chappellaz, J., Davis, M., Delaygue, G., Delmotte, M., Kotlyakov, V.M., Legrand, M., Lipenkov, V.Y., Lorius, C., Pepin, L., Ritz, C., Saltzman, E., Stievenard, M., 1999. Climate and atmospheric history of the past 420,000 years from the Vostok ice core, Antarctica. Nature 399, 429–436.
Philippon, G., Ramstein, G., Charbit, S., Kageyama, M., Ritz, C., Dumas, C., 2006. Evolution of the Antarctic Ice Sheet throughout the last deglaciation: a study with a new coupled climate - north and south hemisphere ice sheet model. Earth and Planetary Science Letters 248, 750–758.
Pollard, D., DeConto, R.M., 2009. Modelling West Antarctic Ice Sheet growth and collapse through the past five million years. Nature 458, 329–U389.
Price, S.F., Conway, H., Waddington, E.D., 2007. Evidence for late Pleistocene thinning of Siple Dome, West Antarctica. Journal of Geophysical Research-Earth Surface 112.
Ramillien, G., Lombard, A., Cazenave, A., Ivins, E.R., Llubes, M., Remy, F., Biancale, R., 2006. Interannual variations of the mass balance of the Antarctica and Greenland Ice Sheets from GRACE. Global and Planetary Change 53, 198–208.
Raynaud, D., Lebel, B., 1979. Total gas content and surface elevation of polar ice sheets. Nature 281, 289–291.
Ritz, C., Rommelaere, V., Dumas, C., 2001. Modeling the evolution of Antarctic Ice Sheet over the last 420,000 years: implications for altitude changes in the Vostok region. Journal of Geophysical Research-Atmospheres 106, 31943–31964.
Rutt, I.C., Hagdorn, M., Hulton, N.R.J., Payne, A.J., 2009. The Glimmer community ice sheet model. Journal of Geophysical Research-Earth Surface 114. doi:10.1029/2008JF001015.
Saito, F., Abe-Ouchi, A., 2010. Modelled response of the volume and thickness of the Antarctic Ice Sheet to the advance of the grounded area. Annals of Glaciology 51, 41–48.
Sasgen, I., Martinec, Z., Fleming, K., 2007. Regional ice-mass changes and glacial-isostatic adjustment in Antarctica from GRACE. Earth and Planetary Science Letters 264, 391–401.
Shapiro, N.M., Ritzwoller, M.H., 2004. Inferring surface heat flux distributions guided by a global seismic model: particular application to Antarctica. Earth and Planetary Science Letters 223, 213–224.
Siddall, M., Milne, G.A., Masson-Delmotte, V., 2011. Uncertainties in elevation changes and their impact on Antarctic temperature records since the end of the last glacial period. Earth and Planetary Science Letters. doi: 10.1016/j.epsl.2011.04.032.
Smith, J.A., Hillenbrand, C.D., Kuhn, G., Larter, R.D., Graham, A.G.C., Ehrmann, W., Moreton, S.G., Forwick, M., 2011. Deglacial history of the West Antarctic Ice Sheet in the western Amundsen Sea embayment. Quaternary Science Reviews 30, 488–505.
Staiger, J.W., Marchant, D.R., Schaefer, J.M., Oberholzer, P., Johnson, J.V., Lewis, A.R., Swanger, K.M., 2006. Plio-Pleistocene history of Ferrar Glacier, Antarctica: implications for climate and ice sheet stability. Earth and Planetary Science Letters 243, 489–503.
Steig, E.J., Fastook, J.L., Zweck, C., Goodwin, I., Licht, K.L., White, J.W.C., Ackert, R.P., 2001. West Antarctic Ice Sheet elevation changes. In: Alley, R.B., Bindshadler, R.A. (Eds.), The West Antarctic Ice Sheet: Behaviour and Environment. AGU, Washington D.C, pp. 75–90.
Stocchi, P., Colleoni, F., Spada, G., 2009. Bounds on the time-history and Holocene mass budget of Antarctica from sea-level records in SE Tunisia. Pure and Applied Geophysics 166, 1319–1341.
Stone, J.O., Balco, G.A., Sugden, D.E., Caffee, M.W., Sass, L.C., Cowdery, S.G., Siddoway, C., 2003. Holocene deglaciation of Marie Byrd Land, West Antarctica. Science 299, 99–102.
Sugden, D.E., Balco, G., Cowdery, S.G., Stone, J.O., Sass, L.C., 2005. Selective glacial erosion and weathering zones in the coastal mountains of Marie Byrd Land, Antarctica. Geomorphology 67, 317–334.
Takada, M., Tani, A., Miura, H., Moriwaki, K., Nagatomo, T., 2003. ESR dating of fossil shells in the Lützow-Holm Bay Region, East Antarctica. Quaternary Science Reviews 22, 1323–1328.
Todd, C., Stone, J., Conway, H., Hall, B., Bromley, G., 2010. Late Quaternary evolution of Reedy Glacier, Antarctica. Quaternary Science Reviews 29, 1328–1341.
Velicogna, I., 2009. Increasing rates of ice mass loss from the Greenland and Antarctic Ice Sheets revealed by GRACE. Geophysical Research Letters 36.
Velicogna, I., Wahr, J., 2006. Measurements of time-variable gravity show mass loss in Antarctica. Science 311, 1754–1756.
Verleyen, E., Hodgson, D.A., Sabbe, K., Vyverman, W., 2004. Late Quaternary deglaciation and climate history of the Larsemann Hills (East Antarctica). Journal of Quaternary Science 19, 361–375.
Verleyen, E., Hodgson, D.A., Milne, G.A., Sabbe, K., Vyverman, W., 2005. Relative sea-level history from the Lambert Glacier region, East Antarctica, and its relation to deglaciation and Holocene glacier readvance. Quaternary Research 63, 45–52.
Vogel, S.W., Tulaczyk, S., Joughin, I.R., 2003. Distribution of basal melting and freezing beneath tributaries of Ice Stream C: implication for the Holocene decay of the West Antarctic Ice Sheet. Annals of Glaciology 36, 273–282.
Waddington, E.D., Conway, H., Steig, E.J., Alley, R.B., Brook, E.J., Taylor, K.C., White, J.W.C., 2005. Decoding the dipstick: thickness of Siple Dome, West Antarctica, at the Last Glacial Maximum. Geology 33, 281–284.
Weaver, A.J., Saenko, O.A., Clark, P.U., Mitrovica, J.X., 2003. Meltwater pulse 1A from Antarctica as a trigger of the Bølling-Allerød warm interval. Science 299, 1709–1713.
Weertman, J., 1964. The theory of glacier sliding. Journal of Glaciology 5, 287–303.
Whitehouse, P.L., Bentley, M.J., Milne, G.A., King, M.A., Thomas, I.D., in review. A new glacial isostatic adjustment model for Antarctica: calibrated and tested using observations of relative sea-level and present-day uplift rates. Geophysical Journal International.
Yamane, M., Yokoyama, Y., Miura, H., Maemoku, H., Iwasaki, S., Matsuzaki, H., 2011. The last deglacial history of Lützow-Holm Bay, East Antarctica. Journal of Quaternary Science 26, 3–6.
Zwartz, D., Bird, M., Stone, J., Lambeck, K., 1998. Holocene sea-level change and ice-sheet history in the Vestfold Hills, East Antarctica. Earth and Planetary Science Letters 155, 131–145.